nature communications

Article

https://doi.org/10.1038/s41467-025-57055-7

Keratinocyte-driven dermal collagen formation in the axolotl skin

Received: 10 July 2024

Accepted: 7 February 2025

Published online: 24 February 2025

Check for updates

Ayaka Ohashi[1], Hirotaka Sakamoto[1], Junpei Kuroda[2], Yohei Kondo[3], Yasuhiro Kamei[4,5,6], Shigenori Nonaka[5,6,7,8], Saya Furukawa[1], Sakiya Yamamoto[1] & Akira Satoh[1]

Type I collagen is a major component of the dermis and is formed by dermal fibroblasts. The development of dermal collagen structures has not been fully elucidated despite the major presence and importance of the dermis. This lack of understanding is due in part to the opacity of mammalian skin and it has been an obstacle to cosmetic and medical developments. We reveal the process of dermal collagen formation using the highly transparent skin of the axolotl and fluorescent collagen probes. We clarify that epidermal cells, not dermal fibroblasts, contribute to dermal collagen formation. Mesenchymal cells (fibroblasts) play a role in modifying the collagen fibers already built by keratinocytes. We confirm that collagen production by keratinocytes is a widely conserved mechanism in other model organisms. Our findings warrant a change in the current consensus about dermal collagen formation and could lead to innovations in cosmetology and skin medication.

The skin is the largest organ of the human body, consisting of two layers: the epidermis and the dermis. The dermis is primarily composed of type I collagen, accounting for 40% of the total protein in the skin[1]. In most tetrapods, dermal collagen cannot be restored to its original fine structure once its structure becomes malformed. Such structural changes cause wrinkles and sagging if caused by aging; however, they can lead to excessive collagen secretion and scar formation, resulting in skin dysfunction, if they occur as a result of skin damage[2]. Therefore, maintaining the normal structure of dermal collagen is important, both cosmetically and medically. Despite the importance of collagen, the process of skin collagen formation in the skin has not been thoroughly elucidated. Clarifying the process of dermal collagen formation is essential for understanding and solving various problems related to skin collagen.

Dermal fibroblasts are considered to play a major role in the formation of extracellular matrix (ECM) by secreting type I collagen, a major component of the dermal ECM structure. The human dermal structure comprises two layers: the papillary dermis and the reticular dermis, and each layer displays specific collagen structures. The papillary dermis has a low-density collagen structure with fragmented fibers arranged in a helical pattern, whereas the reticular dermis has a high-density collagen structure, with fibers woven in a regular and orderly lattice pattern. Maintaining the fine structure in each layer is considered important to keep the skin healthy and beautiful. Although research has been conducted on mature skin[3,4], much remains unknown regarding the construction of dermal collagen.

Axolotls provide an excellent research environment for dermatology, particularly for elucidating the formation of dermal collagen. Much dermatological research has been conducted in vivo and

[1]Graduate School of Environment, Life, Natural Science and Technology, Okayama University, 3-1-1 Tsushima-naka, Okayama 700-8530, Japan. [2]Graduate School of Frontier Biosciences, Osaka University, 1-3 Yamadaoka, Suita, Osaka 565-0871, Japan. [3]Center for One Medicine Innovative Translational Research (COMIT), Nagoya University, 65 Tsurumai-cho, Showa-ku, Nagoya 466-8550, Japan. [4]Laboratory for Biothermology, National Institute for Basic Biology, Myodaiji Nishigo-naka 38, Okazaki, Aichi 444-8585, Japan. [5]The Graduate University for Advanced Studies (SOKENDAI), Myodaiji Nishigo-naka 38, Okazaki, Aichi 444-8585, Japan. [6]Optics and Imaging Facility, Trans-Scale Biology Center, National Institute for Basic Biology, Myodaiji Nishigo-naka 38, Okazaki, Aichi 444-8585, Japan. [7]Laboratory for Spatiotemporal Regulations, National Institute for Basic Biology, Myodaiji Nishigo-naka 38, Okazaki, Aichi 444-8585, Japan. [8]Spatiotemporal Regulations Group, Exploratory Research Center for Life and Living Systems, Myodaiji Nishigo-naka 38, Okazaki, Aichi 444-8585, Japan. e-mail: satoha@cc.okayama-u.ac.jp

in vitro[5–7]. Mature mammalian skin has a thick epidermis and melanocytes, making it difficult to observe the deeper dermis and to detect fluorescent signals in the living state. Human or mouse cultured cells cannot fully mimic dermal collagen structure, despite recent developments in skin-equivalent technology. Axolotl skin has a relatively higher transparency, which aids in research involving the detection of fluorescent signals. Thus, the axolotl is an ideal model animal by which to investigate dermal collagen development.

Research in axolotl skin has been conducted in association with skin regeneration[8–10]. Like that of mammals, the skin of axolotls is composed of epidermis and dermis[11]. The structure of the dermal collagen in axolotls consists of two layers with different structures: the *stratum spongiosum* (SS) and the *stratum compactum* (SC). The SS consists of columnar collagen fibers that extend in the apical-basal direction, whereas the SC has orthogonal lattice-like collagen fibers. Formation of the SC involves cells with lattice-like filopodia in the creation of this collagen structure[12]. The structures within SS and SC can be reconstructed, even after damage. However, there are limits to their regenerative abilities, and the orthogonal lattice-like collagen fiber structure of the SC cannot be completely regenerated after damage in mature axolotls[13]. Moreover, regulation of matrix metalloproteinase (MMP) expression by keratinocytes is crucial for the reformation of collagen structure without scar formation[9]. A study comparing skin regeneration and skin development in the axolotl showed that several similarities exist between regeneration and development[11]. Although axolotl skin and its regeneration have been widely studied, little is known about the detailed mechanism by which the dermal collagen structure is formed. This knowledge is essential for understanding the development of dermal collagen structures in tetrapods and the complete skin regeneration mechanism in axolotls.

In this work, we investigate the transition of dermal collagen structure formation in the axolotl skin dermis using fluorescent probes recently reported by Kuroda et al., 2024[14]. We investigate skin in animals of four different body sizes. We find that keratinocytes secrete collagen and supply it to the dermis, showing a lattice-like collagen structure in smaller animals. In larger animals, lattice-patterned cells and mesenchymal cells participate in the formation of the dermis. The lattice-patterned cells contribute to both collagen production and collagen fiber modification. We also find that the invading mesenchymal cells help separate the upper and lower layers of the axolotl dermal collagen, resulting in the establishment of the three-layered axolotl dermal structure. Finally, we investigate whether collagen production by keratinocytes is a conserved mechanism among species. Collagen production by epidermal cells is confirmed not only in axolotls but also in zebrafish, chickens, and mouse embryos. The conservation of collagen expression by epidermal cells across species indicates that collagen production by epidermal cells is key to the formation of lattice-patterned collagen structures.

Results

Axolotl dermal collagen structure

To elucidate the mature dermal collagen structure of axolotl, we first examined the entire dermal collagen structure of axolotls with a body size of 12 cm (Fig. 1). We used the fluorescent collagen probes DAF-FM DA (hereafter DAF) and DAR-4M (hereafter DAR) to visualize axolotl collagen. These fluorescent probes specifically stain type I, II, and IX collagen and elastin[14]. However, elastin may not be encoded in the reported axolotl genome, and Victoria blue staining for elastin did not generate significant staining in axolotl skin (Supplementary Fig. 1a–e). Furthermore, immunofluorescence for COL2 revealed no COL2 production in the dermis (Supplementary Fig. 1f–h). Because COL9 functions to crosslink COL2[15,16], it is unlikely that COL9 is produced in the absence of COL2. Additionally, we observed a fine overlapping signal between the DAR signal and the GFP signal from TgSceI(mPrrx::GFP-axCOL1a2) transgenic axolotls (Supplementary Fig. 1i). Therefore, we consider that the signals from DAF and DAR are specific to type I collagen as long as we focused on the axolotl skin. Figure 1 shows the results for the mature dermis layer. The collagen structure of the axolotl dermis was seen to be composed of three layers: the two layers of collagen structures (SS and SC) that were previously reported[9,13], and a newly classified layer of collagen structure, named *stratum baladachinum* (SB) (Fig. 1c, d, d3). The SB is located underneath the epidermis (Fig. 1a–d). The structure of the collagen fibers in SC, SS, and SB is shown in Fig. 1d1–d3. SC has a dense, lattice-patterned collagen structure, as previously reported[12] (Fig. 1d1). SS has a low density, and the collagen fibers run in the apical-basal direction (Fig. 1b, d2). SB has a lattice-like structure similar to that of SC (Fig. 1d3). However, the lattice-like structure in SB is less dense and rougher than that of SC. These observations clarify that the axolotl skin structure is composed of three layers–SS, SC, and SB–and that each layer has a characteristic collagen fiber structure.

Development of the dermal collagen structure in axolotls

To investigate the developmental changes of the dermal collagen structure in axolotls, we examined the entire skin collagen fibers using histological staining (Masson's trichrome staining) on limbs of axolotls with a body size ranging from 5 to 12 cm. In the 5-cm-long animals (5 cm dermis), a thin collagen layer was observed beneath the epidermis (Fig. 2a). In the 8-cm-long animals (8 cm dermis), the collagen layer was thicker than that of the 5 cm dermis (Fig. 2b), and cells were observed to be invading in the collagen layer (Fig. 2b). In the 10-cm-long animals (10 cm dermis), we observed the presence of SS-like structures (Fig. 2c). In the 12-cm-long animals (12 cm dermis), mature dermal glands became apparent, and the three-layered structure of SB, SS, and SC could be clearly visualized (Fig. 2d).

Next, we investigated dermal collagen development by immunofluorescent analysis using anti-type I or anti-type III collagen antibodies (Fig. 2e–t). It has been reported that human dermal ECM contains large amounts of type III collagen as well as type I collagen, which plays an important role in maintaining dermis structure[17]. However, the changes in COL3 expression during dermal development have not been fully clarified. In the 5 cm dermis, we observed a single layer of collagen (Fig. 2e, m, q). We named this single collagen layer, which emerges temporarily during dermal collagen development, the *stratum coniunctum*. COL3 signal was observed in the lower basal part of the single collagen layer (Fig. 2i, m, q). Progression to 8 cm dermis resulted in an increase in collagen thickness and the presence of cells within the *stratum coniunctum* (Fig. 2f, n, r). As in the 5 cm dermis, the COL3 signal was found in the lower basal part of the single collagen layer (Fig. 2j, n, r). In the 10 cm dermis, more cells could be observed inside the collagen layer (Fig. 2o, s). At this stage, the separation of the three dermal layers became apparent (Fig. 2g, o, s). We observed that COL3 signals were present not only in the lower basal part of the dermis but also within the SS-like structure (Fig. 2k, o, s). In 12 cm dermis, we observed that the mature dermal collagen structure with fully formed SS, SB, and SC layers (Fig. 2h, p, t). COL3 was present in SS and the layer basal part of SC (Fig. 2l, p, t). Next, we measured the thickness of the dermal collagen layer (Fig. 2u), which confirmed that the thickness of the axolotl dermis increases as the animal develops. These analyses revealed that the axolotl dermal collagen develops from the monolayered structure to the triple-layered structure.

When observing axolotl dermal development, we found that numerous mesenchymal cells were involved in the collagenous structure. We counted the number of nuclei existing in the $COL1^{+}$ collagen layer (Fig. 2v). In the *stratum coniunctum* (5 cm dermis), there were almost no nuclei, but the number of the nucleus was increased as the skin developed. In the electron microscopic observation, we found the cells invading the dermal collagen layer (Supplementary Fig. 2a), where they appeared to digest collagen fibers to integrate the cell body into

https://doi.org/10.1038/s41467-025-57055-7

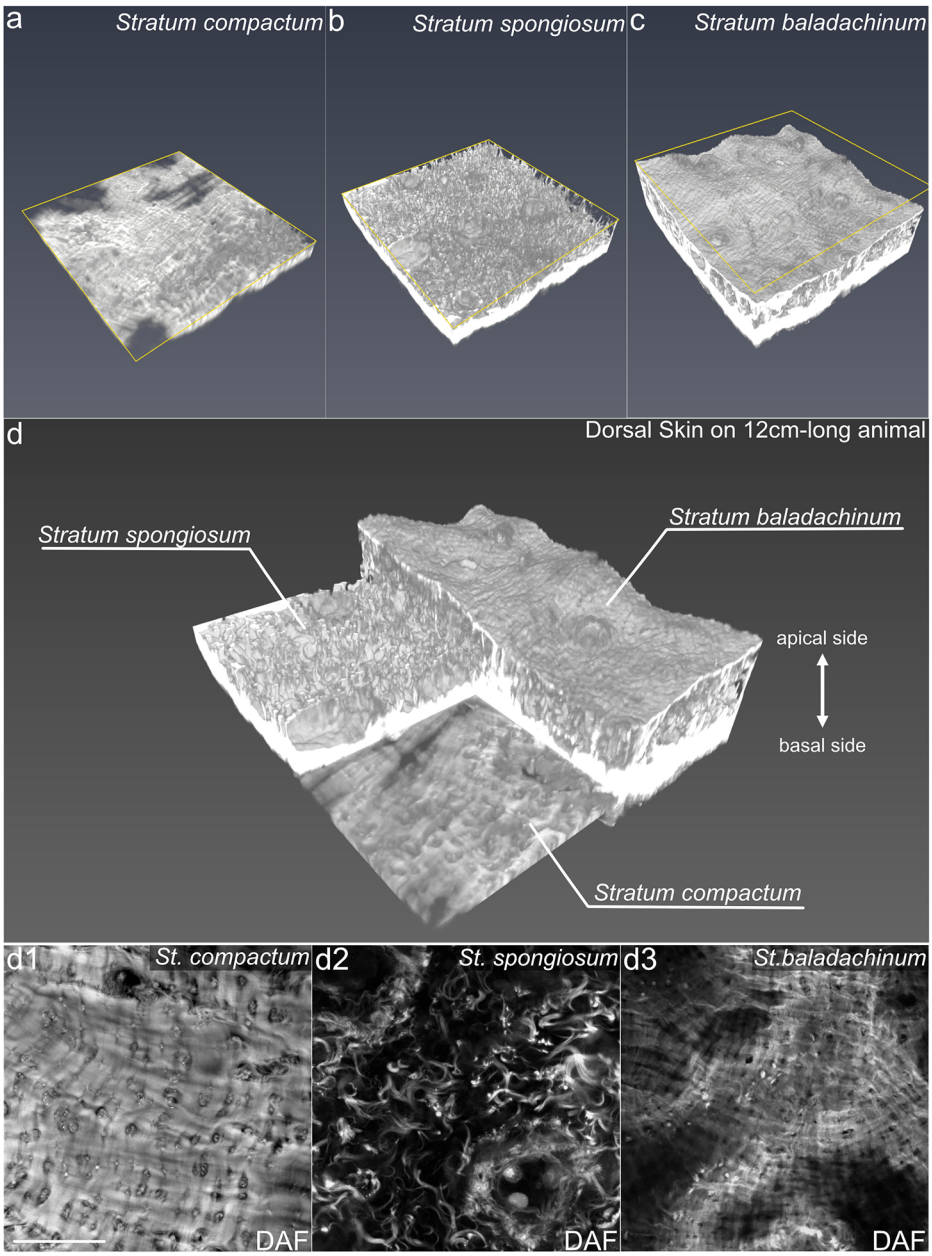

Fig. 1 | Structure of type I collagen in the 12-cm-long axolotl dorsal skin. **a**–**d** DAF was used to label the collagen. The images were taken using a confocal microscope and reconstituted using AMIRA software. Clipping image for visualizing the *stratum compactum* (**a**), *stratum spongiosum* (**b**), and *stratum baladachinum* (**c**). **d** The combined image shows all three layers of the dermal collagen structure in the dorsal skin. **d1**–**d3** Representative images of collagen fibers from the original data taken using confocal microscopy. **d1** *Stratum compactum*, **d2** *stratum spongiosum*, and **d3** *stratum baladachinum*. **d1**–**d3** are the same magnification; the scale bar in **d1** is 50 µm. These collagen structures were confirmed $n = 10$ biologically independent samples. The representative images are shown.

the dermal collagen. This suggests that the mesenchymal cell invasion starts from the 8 cm dermis and settles at the 10 cm dermis stage.

We further confirmed whether the SB was part of the dermal collagen structure or not. We performed double staining for COL1 and COL4, which are components of the basement membrane (Fig. 2w, x). The *stratum coniunctum* and the SB are distinct from the $COL4^+$ basal membrane existing underneath the epidermis (Fig. 2w, w′, x, x′). This indicates that the *stratum coniunctum* and the SB are the newly reported dermal collagen layer existing underneath the basement membrane.

Cells in the axolotl dermal collagen

Dermal collagen structures are known to be formed by dermal fibroblasts. From our previous studies, we identified the dermal fibroblasts that produce the lattice-like collagen structure of the axolotl dermis[12]. These dermal fibroblasts have a characteristic cell morphology with extended lattice-patterned filopodia and are present in the SC. To clarify the changes in the presence of the lattice-patterned filopodia during dermal formation, we visualized filopodia and collagen fibers at each dermal growth stage. We used CMV::GFP transgenics for the filopodia visualization and DAR for collagen visualization. The results are shown in Fig. 3. One layer of *stratum coniunctum* was visible in 5 cm dermis (Fig. 3a, a′), and no GFP signals were detected inside the collagen layer (Fig. 3b, b′). It is noteworthy that the collagen fiber structure of the *stratum coniunctum* in the 5 cm dermis had a lattice structure, even though no lattice-patterned filopodia were found (Fig. 3b, b′). Similar to the results shown in Fig. 2, we detected penetration of mesenchymal cells into the collagen layer in the 8 cm dermis

https://doi.org/10.1038/s41467-025-57055-7

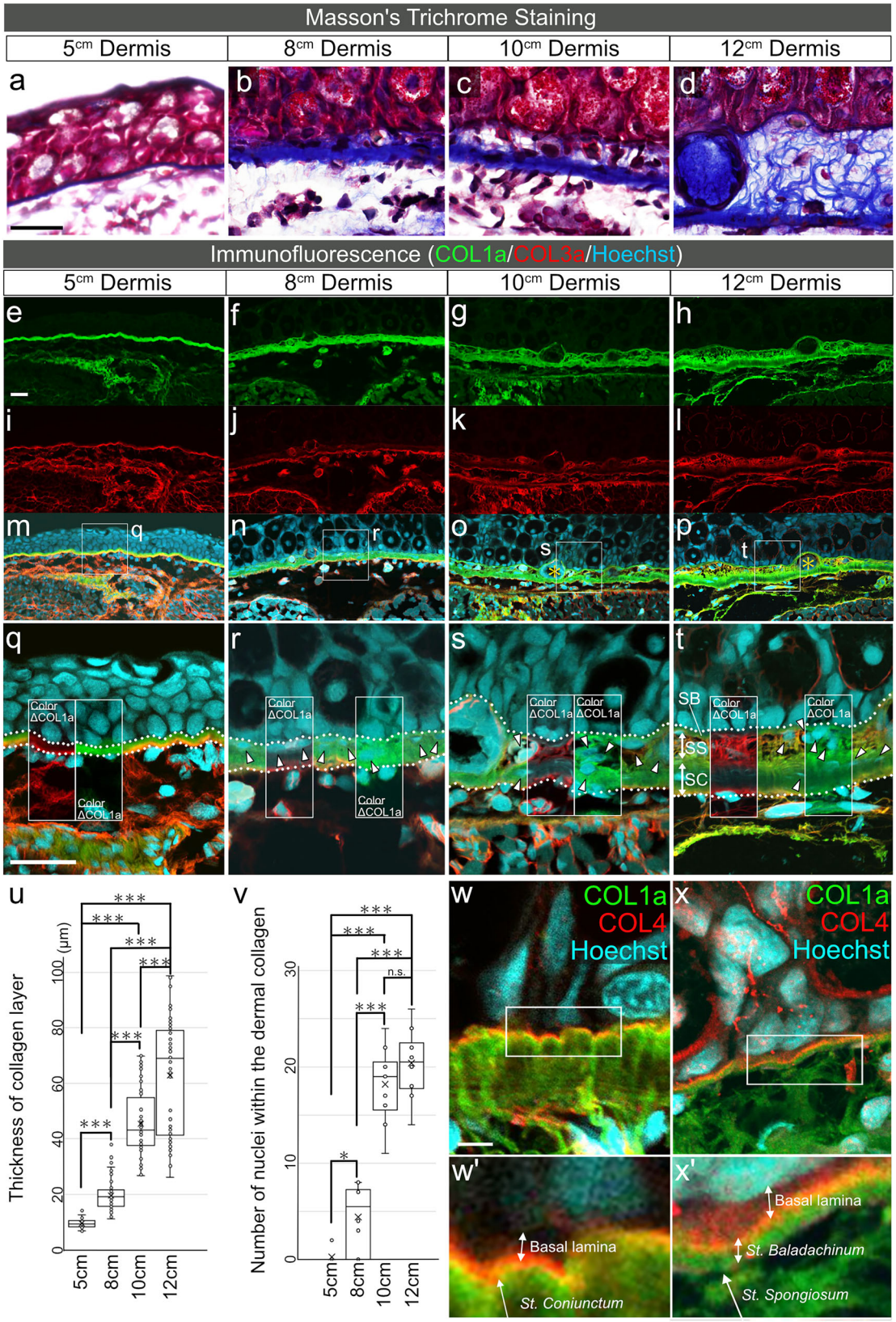

(Fig. 3c, c′). The presence of filopodia was evident in the 8 cm dermis (Fig. 3d, d′). The 10 cm dermis comprised pre-mature SC, SS, and SB structures (Fig. 3e, e′). Moreover, consistent with the results shown in Fig. 2, cell invasion between the SC and SB was seen (Fig. 3e, e′). Compared to the mature SB in the 12 cm dermis (Fig. 1), the SB in the 10 cm dermis had a thinner and rougher structure (Fig. 3f). In the SS, collagen fibers formed in the apical-basal orientation around the cells (Fig. 3g). In the SC of the 10 cm dermis, lattice-patterned filopodia were clearly visible (Fig. 3h, h′). In the 12 cm dermis, the three mature layers of SS, SB, and SC were found (Fig. 3i, i′), and cells were abundant in the SS (Fig. 3k, i′). The SB is lattice-patterned collagen fiber and has a more robust structure compared to the 10 cm dermis (Fig. 3j). Lattice-

https://doi.org/10.1038/s41467-025-57055-7

Fig. 2 | Development of dermal collagen structure during growth. **a**–**d** Histological observation of the axolotl dorsal skin. Masson's trichrome staining was performed for 5 to 12 cm dermis. Blue indicates collagen, red indicates cytoplasm, and dark brown color indicates nuclei. **e**–**t** Immunofluorescence of **e**–**h** COL1a (green), **i**–**l** COL3 (red), and nucleus (Hoechst 33342; blue) in the axolotl dermis. **m**–**p** Merge images of (**e**–**l**). **q**–**t** High magnification view of the boxed region in (**m**–**p**). SB, SS, and SC indicate *stratum baladachinum, stratum spongiosum*, and *Stratum compactum*. The open windows in **q**–**t** display views with one color deleted. For example, ΔCOL1a indicates that the green signal of COL1a is omitted from the region. The expression patterns were confirmed in five independent samples at each time point, and the representative images are shown. **u** Analysis of thickness of collagen layer ($n = 4$ biologically independent samples) Each point on the box plot represents all measured data points. p values from up to down: 1.40 e^{-37}, 3.10 e^{-42}, 2.91 e^{-32}, 2.60 e^{-9}, 4.92 e^{-34}, 2.72 e^{-30}. **v** Counting the number of nuclei in the dermis ($n = 4$ for 5 cm, and $n = 5$ for 8, 10, and 12 cm biologically independent samples) Each point on the box plot represents all measured data points. p values from up to down: 1.63 e^{-10}, 3.74 e^{-9}, 3.11 e^{-8}, 1.16, 6.28 e^{-7}, 0.025. **w** Immunofluorescence of COL1a (green), COL4 (red), and nucleus (Hoechst 33342; blue) of the *stratum coniunctum*. **w'** High magnification view in w. x Immunofluorescence of COL1a (green), COL4 (red) and nucleus (Hoechst 33342; blue) of the 12 cm. **x'** High magnification view in x. The scale bars in (**a**, **e**, **q**) are 50 μm, and that in w is 10 μm. **a**–**d**, **e**–**o**, **q**–**t**, and **w**–**x** are the same magnification. The expression patterns were confirmed in five independent samples at each time point, and the representative images are shown. The white dotted line in **q**–**t** indicates the dermal collagen layer. The statistical analysis was performed using two-tailed ANOVA, followed by pairwise two-tailed t-tests with Bonferroni correction. $^{*}p < 0.05$, $^{**}p < 0.025$, $^{***}p < 0.01$. n.s. no significant difference. Each box represents the interquartile range (IQR, the range between the 25th and 75th percentile) with the mid-point of the data, bars indicate the upper and lower value within 1.5 times the IQR. Source data are provided as a Source Data file.

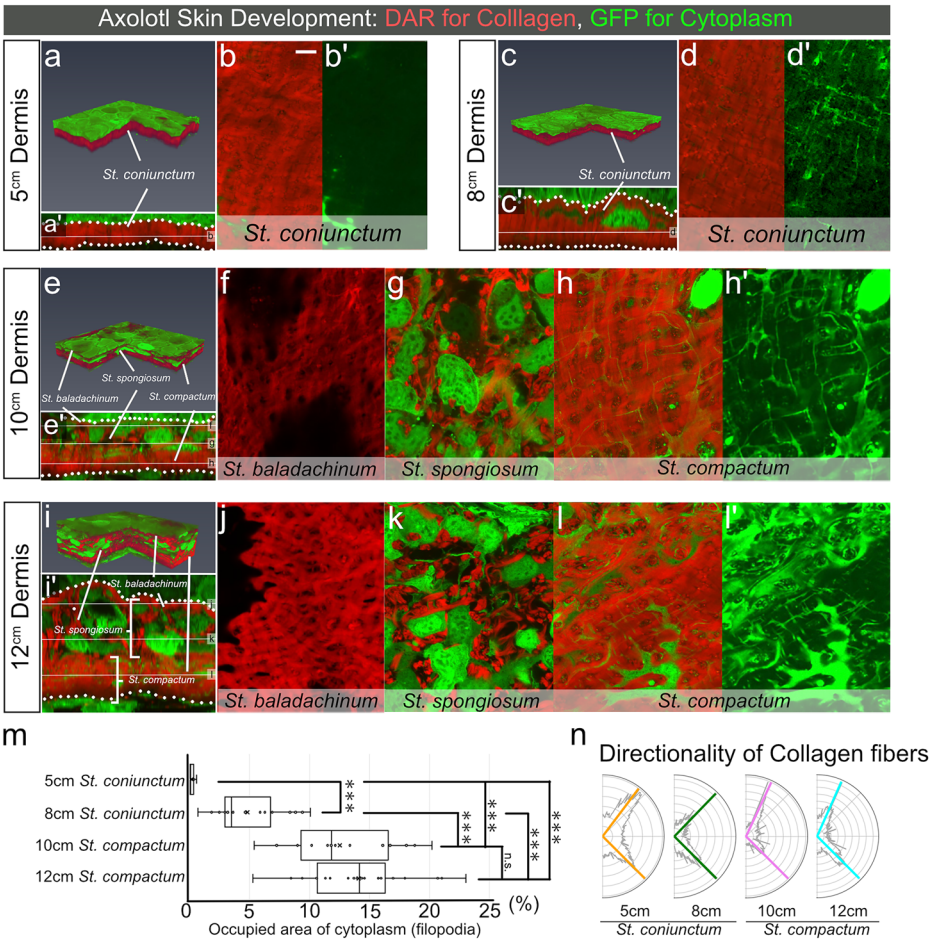

Fig. 3 | Developmental changes of entire collagen structure and collagen fibers at each stage. The red color indicates collagen, and the green color is for cytoplasm. **a**–**f** The structure of collagen fibers and the presentation of cytoplasm on *stratum coniunctum* at 5 cm and 8 cm dermis. **a**, **c** Three-dimensional (3D) structure. **a'**, **c'** Orthogonal image from the reconstituted images. **b**, **d** The merged image of collagen fibers and cytoplasm. **b'**, **d'** Cytoplasm. **e**–**l** The structure of collagen fibers and the presentation of cytoplasm on three collagen layers (*stratum baladachinum*, *stratum spongiosum*, *stratum compactum*) at 10 and 12 cm dermis. **e**, **i** 3D structure. **e'**, **i'** Orthogonal image from the reconstituted images. **f**, **j** The structure of collagen fiber in *stratum baladachinum*. These images are the maximum intensity projection. **g**, **k** The structure of collagen fiber and the location of cytoplasm at the *stratum spongiosum* and **h**, **l** *stratum compactum*. **h'**, **l'** Cytoplasm. The expression patterns were confirmed in five independent samples at each time point, and the representative images are shown. **m** Quantification of occupied area of cytoplasm (filopodia) ($n = 3$ biologically independent samples.) Each point on the box plot represents all measured data points. p values from left to right: 1.89 e^{-6}, 1.59e^{-5}, 6.20e^{-8}, 1.66, 4.17 e^{-9}, 6.36 e^{-12}. **n** Analysis of directionality of collagen fibers. The same analysis was performed on five biologically independent samples, and the representative pattern was selected and presented. The scale bars in **b** is 10 μm. All images have the same magnification. The white line in **a'**, **c'**, **e'**, **i'** indicate the dermal collagen layer. The statistical analysis was performed using two-tailed ANOVA, followed by pairwise two-tailed t-tests with Bonferroni correction. $^{*}p < 0.05$, $^{**}p < 0.025$, $^{***}p < 0.01$. n.s. no significant difference. Each box represents the interquartile range (IQR, the range between the 25th and 75th percentile) with the mid-point of the data, bars indicate the upper and lower value within 1.5 times the IQR. Source data are provided as a Source Data file.

patterned filopodia were found in the SC (Fig. 3l, l'), and we conducted a quantitative evaluation of their proportion (Fig. 3m). A large number of filopodia were quantified in 10 and 12 cm dermis, whereas fewer were observed in the 8 and 5 cm dermis, especially in the latter (Fig. 3m). Moreover, we analyzed the directionality of collagen fibers at each stage in the SC and in the *stratum coniunctum* (Fig. 3n). Directionality analysis revealed that the collagen structures in both the *stratum coniunctum* and SC exhibited bipolarity (Fig. 3n). These observations suggested that lattice-patterned fibroblasts appeared in the 8 cm dermis; therefore, despite their absence in the 5 cm dermis, the collagen structure is lattice-patterned. This suggests that cells other than lattice-patterned cells are involved in forming the lattice-patterned collagen structure.

We performed a detailed investigation of ultrastructure using electron microscopy (EM) in 8 cm dermis and 12 cm dermis. (Supplementary Fig. 3). Using TEM imaging, we confirmed the typical collagen structure as previously reported[18,19]. In the 8 cm dermis, mesenchymal cells could be observed invading the *stratum coniunctum* with filopodia (Supplementary Fig. 3a), with orthogonal collagen fibers (Supplementary Fig. 3b). The filopodia of the cells were seen to be inserted between these longitudinally and transversely orthogonal collagen fibers (Supplementary Fig. 3b). In 12 cm dermis, EM confirmed that the collagen lattice structure in SB and SC was composed of orthogonal collagen fibers (Supplementary Fig. 3c–e). In addition, the thickness of each fiber in the SB and SC was different (Supplementary Fig. 3d, e). These findings suggest that the *stratum coniunctum*, SB, and SC have orthogonal fiber structures, but SB and SC have slightly different microfiber structures.

We then focused on cell invasion into the collagen layer. As shown in Figs. 2, 3, the invasion of mesenchymal cells in the dermis appeared to be a key step in SS formation. It was not clear how the cells, whether entering or inserting filopodia, interacted with the densely woven collagen layer to achieve entry and filopodia insertion. We focused on the expression of genes encoding collagen-degrading enzymes, specifically *Mmp 1, 2, 9, 13*, and *14*, which have type I collagen-degrading activity. We investigated the expression of these genes (Supplementary Fig. 4a–d, a'–d') and observed *Mmp2*$^+$ cells and *Mmp9*$^+$ cells at all stages from 5 to 12 cm dermis, either within the dermis or just beneath it (Sup. Fig. 4a2, b2, c2, d2, a3, b3, c3, d3). Additionally, *Mmp13*$^+$ cells were found at 12 cm dermis (Sup. Fig. 4d4). These results suggest that cells invade the collagen layer while degrading type I collagen. Previous studies have shown that inhibition of cell invasion during the skin regeneration process in the axolotl results in inhibition of SS formation[11]. As the regenerative process mimics the developmental process, it was speculated that cell invasion inside the collagen layer is involved in the formation of SS in the developmental process.

Type I collagen production in keratinocytes

As can be seen in Fig. 3, a lattice-patterned collagen structure was identified despite the absence of lattice-patterned fibroblasts in the 5 cm dermis. This suggests that cells other than lattice-patterned fibroblasts contribute to the formation of lattice-patterned collagen structures in the 5 cm dermis. To identify the cells that contribute to dermal collagen formation, we conducted in situ hybridization to clarify the *Col1a1* expression pattern at each stage (Fig. 4a–d). *Col1a1* signals were found not only in the mesenchymal cells but also in the keratin (KRT)-positive epidermal cells in the basal layer of the epidermis in the 5 and 8 cm dermis (Fig. 4a, a', b, b'). Conversely, in 10 and 12 cm dermis, keratinocytes displayed no strong *Col1a1* signals, whereas cells in the SS and SC exhibited intense *Col1a1* expression (Fig. 4 c, c', d, d'). In mammals, keratinocytes are not typically associated with the production of type I collagen[20,21]. Therefore, we further investigated whether protein synthesis from the *Col1a1* mRNA in keratinocytes was inhibited by post-translational regulation. For this purpose, we conducted immunofluorescence staining using pro-type I collagen antibodies (Fig. 4e–h, e'–h') and IEM (Fig. 4i–k). Briefly, pro-type I collagen (procollagen) can be detected prior to collagen secretion from a cell and just before fiberization[22]. By using the anti-procollagen antibody, we could identify the location of the collagen molecules within the cell and the region where new collagen was being fiberized. Procollagen signals were detected in the keratinocytes in the 5, 8, and 10 cm dermis (Fig. 4e–g). In particular, we identified a stronger signal on the apical side of the dermis in the 5 to 10 cm dermis. Figure 4e'–h' shows a heatmap of all stages. A strong signal was observed on the epidermal cell side (Fig. 4e', f'), suggesting that collagen is secreted from epidermal cells. Procollagen expression patterns in the 10 and 12 cm dermis suggest that collagen supply is from cells in the SS and that collagen production rate is decreased by the 12 cm dermis stage. In the 12 cm dermis, relatively weaker procollagen signals were present in keratinocytes and the apical side of the SB (Fig. 4h). Furthermore, the integrated heatmap combining multiple images also produced similar findings in 5 cm dermis to 12 cm dermis (Supplementary Fig. 5a–d). We further confirmed these observations using the 5 cm dermis using IEM (Fig. 4i–k). IEM signals were detected in the basement membrane (*lamina lucida*) (Fig. 4i, i'). IEM signals could also be observed in the mesenchymal cell just below the dermal collagen layer (Fig. 4j, j'). In the absence of primary antibodies (negative control), no IEM signals were observed (Fig. 4k, k'). These results suggest that collagen is secreted from keratinocytes and delivered to the dermis through the basement membrane.

To determine how collagen produced by keratinocytes contributes to the formation of dermal collagen structures, we conducted a pulse-chase experiment using DAR and DAF (Fig. 5a). DAR was injected under the skin on the dorsal side of the forelimb, and the injected animals were kept for 5 days. Then, DAF was injected into the area where the red fluorescence from DAR was visible. We collected the skin 1 day after the DAF injection. Consequently, most collagen fibers had both red and green fluorescence, whereas green signals were found only in newly synthesized collagens that were made between the day of the DAR injection and the day of the DAF injection (within 5 days). The skin was analyzed using a confocal microscope. On the apical side, DAF signals occupied a larger area than DAR signals (Fig. 5b). In the basal side, DAF and DAR signals were almost completely overlapping (Fig. 5c). To visualize the spatial occupancy, we reconstituted the confocal images, resulting in an orthogonal image (Fig. 5d), which clearly demonstrated that the newly synthesized collagen fibers were located at the apical side of *stratum coniunctum*. To visualize this quantitatively, we made a histogram of Fig. 5d and calculated the rate of each color (Fig. 5e, f). Whereas most of the apical side contained new collagen (DAF$^+$), the area of DAR and DAF gradually equalized as it shifted toward the basal side. We conducted another analysis to quantify the areas of DAR and DAF in all sections (Fig. 5g). The area of DAF was significantly larger than that of DAR (Fig. 5g). To confirm that the offset of the DAR/DAF labeling is not caused by difference in diffusion properties or tissue specificity, we conducted two control experiments. First, we reversed the injection timing of DAR and DAF in the 5 cm dermis, left it for 10 days and performed the same analysis (Supplementary Fig. 6). As in Fig. 5, only new collagen (DAR$^+$) signals were observed on the apical side of the dermis (Supplementary Fig. 6a–e), indicating that the stacking on the apical side is not affected by the difference in the diffusion properties of the dyes. Next, we performed a pulse-chase experiment on tendons in order to test whether tissue specificity caused the offset of the DAR/DAF labeling (Supplementary Fig. 6f). As a result, in tendons, new collagen (DAF$^+$ fibers) was observed within old collagen (DAR$^+$ fibers), and the offset of DAR/DAF was observed among the older collagen fibers (Sup. Fig. 6f1–3). This indicates that the pulse-chase analysis using DAR and DAF accurately monitors newly synthesized collagen fibers regardless of tissues. The accuracy and the results of the pulse-chase analysis in the axolotl skin confirm that the newly synthesized collagen

https://doi.org/10.1038/s41467-025-57055-7

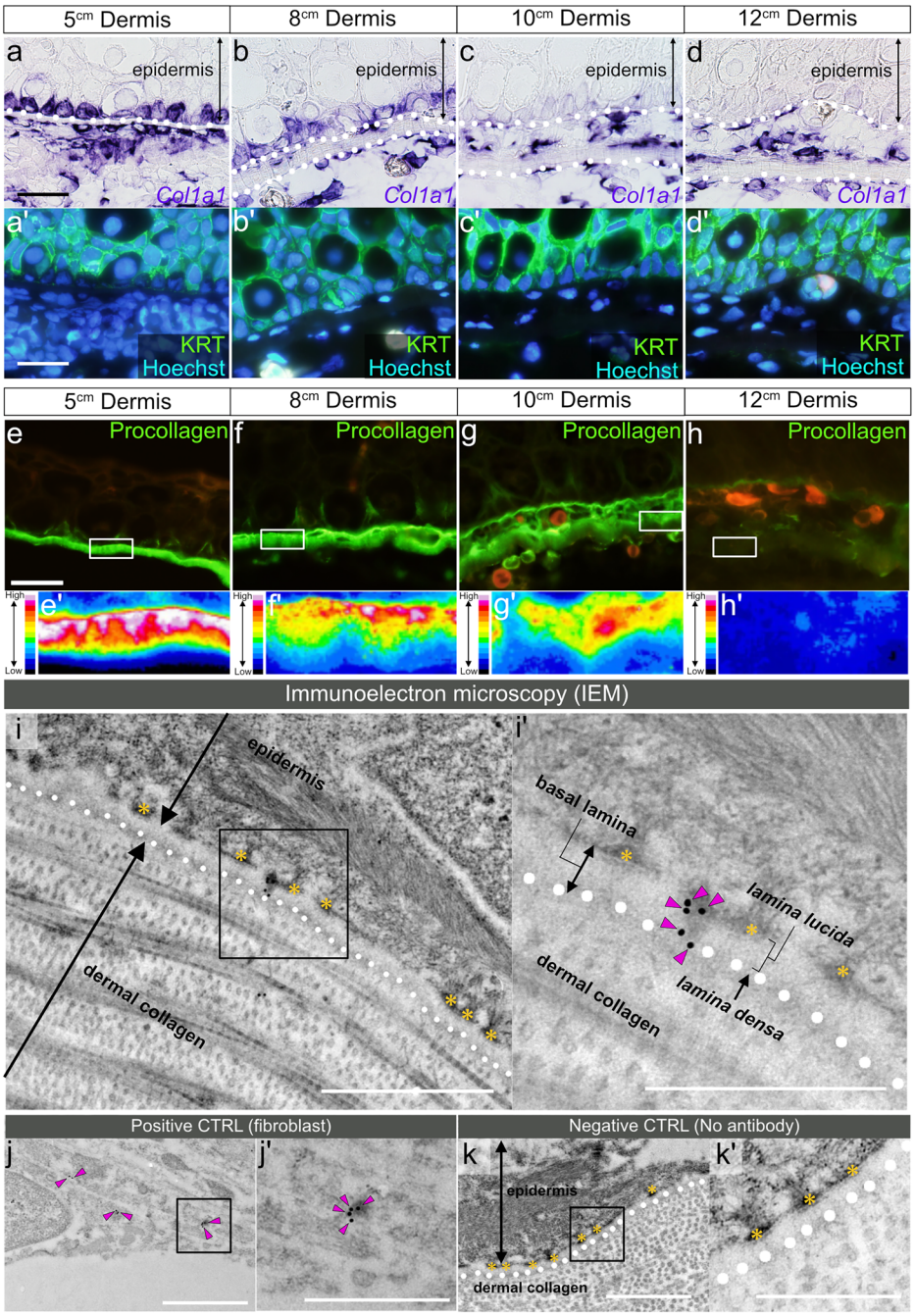

Fig. 4 | Type I collagen production in keratinocytes. a–d The *Col1a1* expression pattern in the dorsal skin was revealed by in situ hybridization. **a'–d'** Immunofluorescence of pan-cytokeratin (KRT) and Hoechst signal (nucleus). **e–h** Procollagen expression from the 5 cm dermis to the 12 cm dermis. **e'–h'** The heatmap shows the signal strength of the boxed region in (**e–h**). The expression patterns were confirmed in five independent samples at each time point, and the representative images are shown. Heatmap analysis was performed on three selected biologically independent samples from $n = 5$, and a representative example is presented. **i–k** Immunoelectron microscopy (IEM) using procollagen antibody. **i'** Higher magnification views of the boxed region in (**i**). Arrowheads indicate the signals from the basement membrane (*lamina lucida*). **j, j'** Positive control. Showing collagen production in mesenchymal cells. **j'** The high magnification view of the boxed region in (**j**). The pink arrowheads indicate the IEM signals from in the mesenchymal cells. **k, k'** Negative control (no antibody). **k'** The high magnification view of the boxed region in (**k**). Yellow asterisks indicate the hemidesmosomes. The white dotted line indicates the basement membrane (*lamina densa*). The scale bars in **a**, **a'**, **e** are 50 μm, those in **i**, **j**, **j'**, **k**, **k'** are 1 μm, and that in **i'** is 500 nm. More than 20 IEM images were collected from the three biologically independent samples. And the representative images are shown.

layers are stacked on the epidermal side. Considering that neither mesenchymal cells nor lattice-patterned fibroblasts were present at the 5 cm dermis as shown in Figs. 2, 3, these results suggest that the collagen structure formation at the 5 cm dermis was due to collagen production by keratinocytes only.

A basement membrane exists between the epidermis and dermis. When considering the supply of collagen from the epidermis, the presence of the basement membrane is notable. The results of immunofluorescence staining for the basement membrane component laminin are shown in Supplementary Fig. 7. Signals of laminin were observed just beneath the epidermis from 5 to 12 cm dermis (Supplementary Fig. 7a–d). We investigated the ultrastructure of the basement membrane using an EM (Supplementary Fig. 7e); hemidesmosomes and basal lamina composed of *lamina densa*, and *lamina*

https://doi.org/10.1038/s41467-025-57055-7

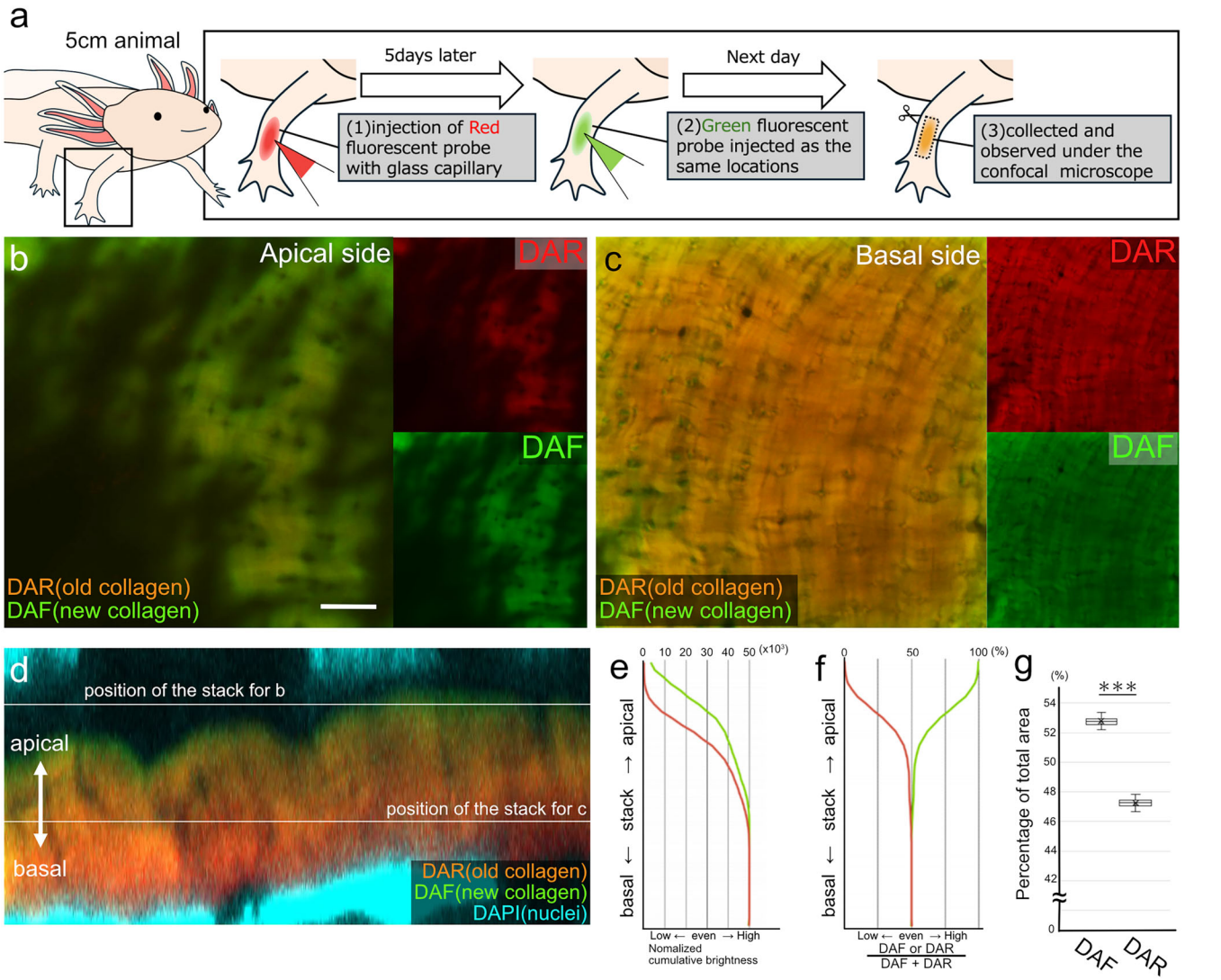

Fig. 5 | Structural changes of dermal collagen conducted by keratinocytes. **a** Schematic diagram of the experiment. (1) Injection of DAR under the dorsal skin (Day 0). (2) DAF is injected at the same locations as DAR on Day 5. (3) Samples were harvested on Day 6. **b**–**d** Confocal microscopic images: **b** epidermis side, **c** hypodermis side, **d** orthogonal image from the reconstituted images. The results were confirmed in four independent samples. **e** Histogram of DAR and DAF areas from all stack images. **f** Histogram of the rate of each color. The same analysis was performed on four biologically independent samples, and the representative histograms are shown. **g** Percentage of the area of DAR and DAF ($n = 4$ biologically independent samples). p values = 3.48 e^{-6}. The scale bars in **b**, **c** are 10 µm. The statistical analysis was performed using t-tests (two-tailed). ***$p < 0.01$. n.s. no significant difference. All images are the same magnification. Each box represents the interquartile range (IQR, the range between the 25th and 75th percentile) with the mid-point of the data, bars indicate the upper and lower value within 1.5 times the IQR. Source data are provided as a Source Data file.

lucida was also observed. Furthermore, we found some areas showing hole-like structures on EM (Supplementary Fig. 7e). It has been reported that holes exist in the basal membrane in Drosophila developmental stages and early mouse embryos[23,24]. Our results suggest that holes may also exist in the basement membrane of the developing stage of the axolotls. It has been reported that COL4 in the axolotls is partially absent[25]. It is also possible that the basement membrane of the axolotls may have a very rough structure compared with that of mammals. These observations support the idea that collagen molecules produced by keratinocytes are transported to the dermis through the basement membrane.

Transition of dermal collagen structure through each developmental stage

Our results demonstrate that keratinocytes, in addition to dermal fibroblasts, are a new type of collagen-producing cell in the early stages of dermal formation (5 cm dermis), responsible for creating the initial lattice-patterned collagen structure. Next, to elucidate how collagen production by dermal cells and keratinocytes cooperatively contributes to dermis formation, we conducted a DAR/DAF pulse-chase experiment similar to that depicted in Fig. 5a in four phases: from 5 to 8 cm dermis, 8 to 10 cm dermis, 10 to 12 cm dermis, and 5 to 12 cm dermis. In the dermis development from 5 to 8 cm dermis, accumulation of new collagen on the apical side could be observed (Fig. 6a, b). The collagen fibers that were generated at the 5 cm dermis (DAR^+ fibers in Fig. 6a) were located basally in the 8 cm dermis (Fig. 6b, c1–c3). We also found that there are many pillar-like formations (Fig. 6a′, c1′) with only a DAF signal, indicating that the pillar formation takes place in a stage after 5 cm dermis. These pillars, which are formed by fibroblasts having a pillar-like filopodia, have been reported previously[12]. It is likely that *Col1a1*$^+$ cells located on the mesenchymal side, as shown in Fig. 4a, b, may contribute to the formation of this pillar-like structure. From 8 to 10 cm dermis, the DAF signals were also detected on the apical side (Fig. 6d, e). The SB-like structure had only a DAF signal,

https://doi.org/10.1038/s41467-025-57055-7

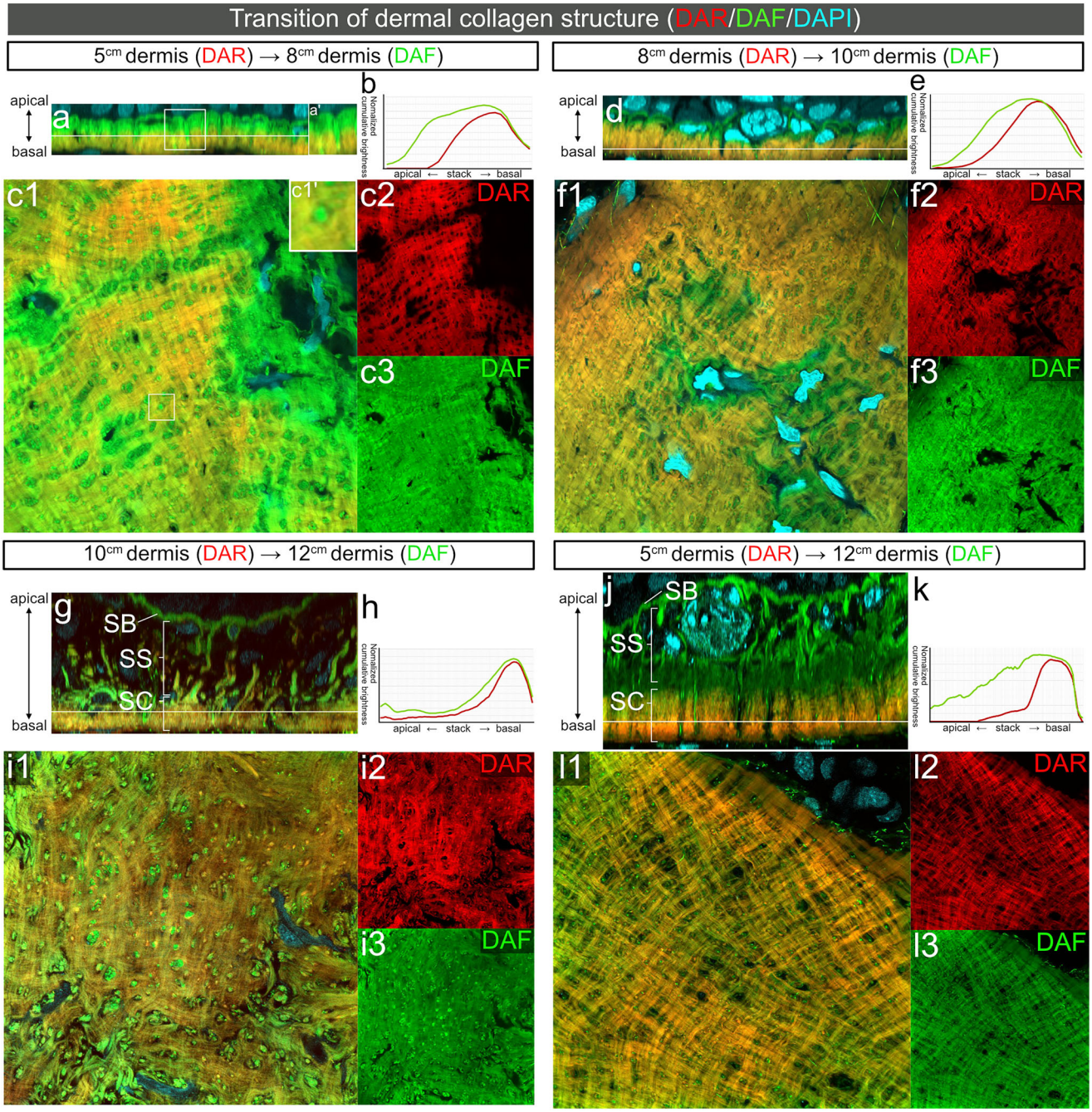

Fig. 6 | Dynamics of dermal collagen formation during growth. a–l Changes in collagen structure from 5 to 8 cm dermis, 8 to 10 cm dermis, 10 to 12 cm dermis, and 5 to 12 cm dermis. **a**, **d**, **g**, **j** Orthogonal images from the reconstituted confocal images. **b**, **e**, **h**, **k** Histograms of DAR and DAF areas from all stacked images. **c1–c3**, **f1–f3**, **i1–i3**, **l1–l3** Representative fiber images at the basal side of the dermis. The scale bars in **c** is 20 µm. All images are the same magnification. SB, SS, and SC indicate *stratum baladachinum, stratum spongiosum*, and *Stratum compactum*. The experiment confirmed five biologically independent samples at each time point. The representative histograms and images are selected and shown from the five samples. Source data are provided as a Source Data file.

indicating that the SB was composed of newly synthesized collagen between 8 and 10 cm dermis (Fig. 6d, e). However, older collagens (DAR^+) could be observed in the SC, indicating that the collagen fibers synthesized at the 8 cm dermis contributed to the SC of the 10 cm dermis (Fig. 6d, f1–f3). Focusing on the hypodermis side of the SC, the DAF^+ area seemed to be slightly larger than that of the DAR^+ area (Fig. 6f1–f3), suggesting that new collagen fiberization takes place in the SC. From 10 to 12 cm dermis, the DAF signal was detected apically (Fig. 6g, h), and many cells were observed within the SB. This suggests that SS and SB is formed by cells that have invaded the collagen layer. In contrast, collagen produced at 10 cm dermis (DAR^+) was present in the SC (Fig. 6g–i). In the lattice structure of the SC were DAF–only collagen fibers (Fig. 6h, i1–i3). This means that new collagen fibers appeared inside the SC. In particular, many filopodia of lattice-patterned cells were observed at 8 to 12 cm dermis, which is due to collagen production by lattice-patterned cells. Finally, changes from 5 to 12 cm dermis are shown in Fig. 6j–l. Structures formed at 5 cm dermis (DAR^+ fibers) were found to form the basal layer (basal side) of the 12 cm dermis at the SC (Fig. 6j–l). Additionally, the structure from 5 cm dermis collagen fibers (DAR^+ fibers) appears to be in a low-density

state (Fig. 6l1–l3). These results suggest that the lattice-patterned collagen structure initially synthesized by keratinocytes becomes the SC and undergoes fine changes during growth.

Since lattice-patterned cells have been shown to contribute to the formation of lattice collagen in SC[12], we hypothesized that these cells induce subtle structural changes in SC. In line with previous findings, we observed cells with filopodia within the SC (Supplementary Fig. 8a, b). Additionally, secreted collagen with a lattice pattern was evident (Supplementary Fig. 8c, d). We closely examined pulse-chase experiments conducted in the dermis. The results of subtracting the red (older collagen) color from the green (newly synthesized collagen) color are displayed in Supplementary Fig. 8e, f, confirming the independent existence of green fibers (DAF^+ fibers). This suggests that the mesenchymal cells, including the lattice-patterned cells, contribute to building up the preexisting collagen fibers.

To confirm whether the preexisting fibers became thicker during skin development at the single fiber level, we used EM to investigate changes at the single fiber level in 5 cm dermis, in which filopodia are absent, and in 12 cm dermis, in which filopodia are present. The entire collagen ultrastructure at 5 cm dermis is shown in Fig. 7a. No cells or filopodia were detected inside the collagen layer (Fig. 7a). Fig. 7b shows the structure just below the keratinocytes, and Fig. 7c, d shows the ultrastructure of the 12 cm dermis. The SB can be observed just below the keratinocytes, and the single collagen fiber is very thin (Fig. 7c). SC collagen fibers are shown in Fig. 7d; the collagen fibers comprising SC were thicker than those comprising SB. In addition, filopodia of lattice-patterned cells were detected inside the SC as if they were inserted between the fibrous layers (Fig. 7d). We measured the area of the single collagen fiber in the 5 cm dermis and the single fiber of SC at the 12 cm dermis (Fig. 7e); the single collagen fiber at 12 cm dermis was significantly thicker than that in the 5 cm dermis. These results suggest that the collagen supplied by lattice-patterned cells thickens the single collagen fiber, forms new fibers, and, as a result, modifies the SC structure.

Transition of collagen fibers in the axolotl dermis

We found that lattice-patterned cells expand filopodia and provide collagen to modify the SC collagen structure. The previous study reported that the lattice-patterned cells secrete collagen around the expanded lattice-patterned filopodia[12]. We succeeded in further elucidating the role of the lattice-patterned cells in the axolotl dermis. The lattice-patterned filopodia are inserted into the existing collagen layer (Fig. 7d), and collagen molecules are secreting around the filopodia, modifying and building up the collagen fibers (Fig. 7 and Supplementary Fig. 8e, f). This causes slight differences in the lattice-patterned collagen structure. Such modification may cause a transition of the dermal collagen fibers. To test and visualize this transition of the collagen fibers, we performed principal component analysis (PCA). Properties of the fibers involved in lattice-patterned cells were subjected to PCA with features derived using a pretrained deep-learning model (Fig. 8). We analyzed seven lattice fiber structures (5, 8, 10 cm: SS side of SC (10 cm Spo), 10 cm: hypodermis side of SC (10 cm hypo), 12 cm: SS side of SC (12 cm spo), 12 cm: hypodermis side of SC (12 cm hypo)) (Fig. 8a). Feature extraction from our collagen images, we adopted ResNet, which is one of the best-tested models for image recognition and that has been used on biological data for feature extraction[26–28]. Each fiber group occupied specific domains in the PCA plot (Fig. 8b, c). The one-dimensional PCA scores plot in PC1 suggested

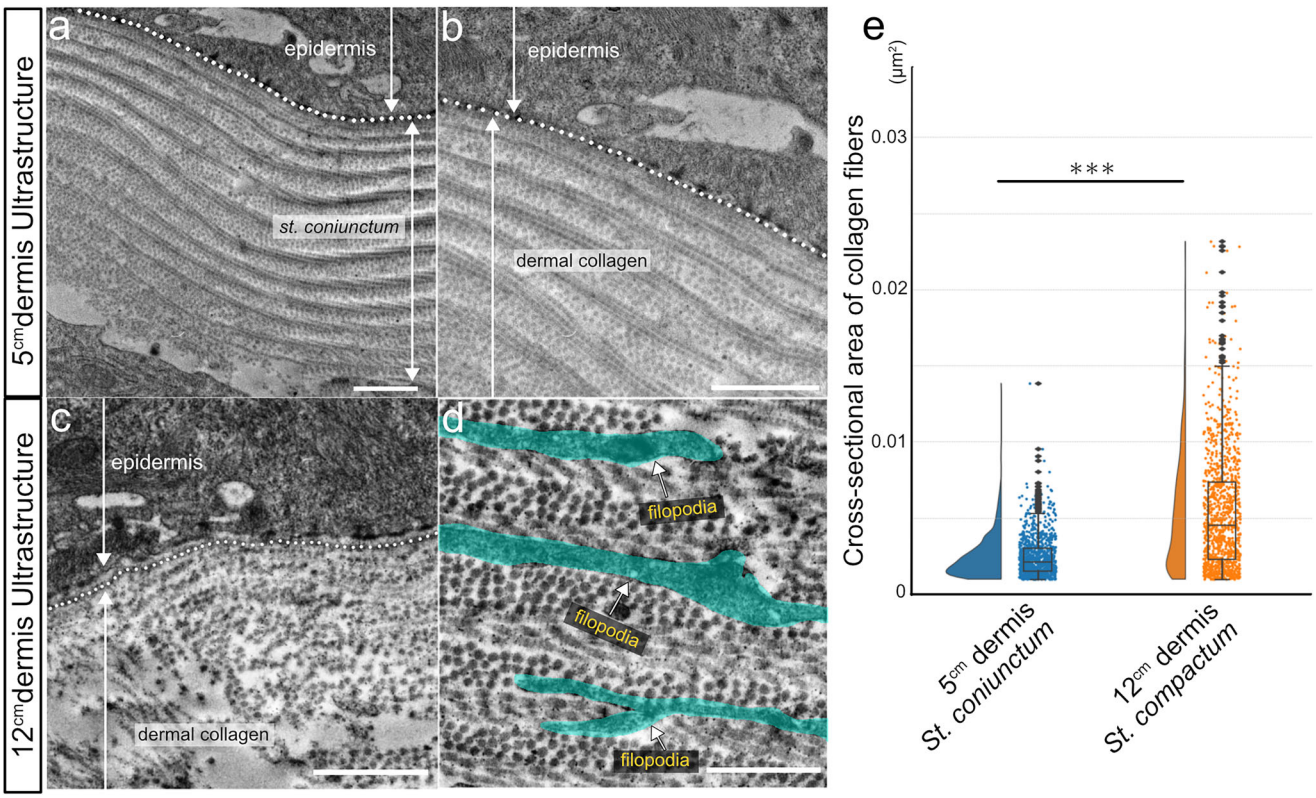

Fig. 7 | Changes in collagen fiber in the dermis development. a, **b** Ultrastructure of 12 cm dermis. **a** Keratinocyte and collagen fibers in the *stratum baladachinum*. **b** Collagen fibers in the *stratum compactum*. **c**, **d** Ultrastructure of 5 cm dermis. **c** Keratinocyte and collagen fibers in the *stratum coniunctum*. **d** Epidermis side of the *stratum coniunctum*. **e** Analysis of the size of collagen fibrils ($n = 3$ biologically independent samples). Each point on the box plot represents all measured data points. p values: $2.83\ e^{-99}$. The statistical analysis was performed using t-tests (two-tailed). $^{***}p < 0.01$. The representative images were selected from 15 images made from three independent samples. The scale bars in (**a**–**d**) are 1 μm. Each box represents the interquartile range (IQR, the range between the 25th and 75th percentile) with the mid-point of the data, bars indicate the upper and lower value within 1.5 times the IQR. Source data are provided as a Source Data file.

https://doi.org/10.1038/s41467-025-57055-7

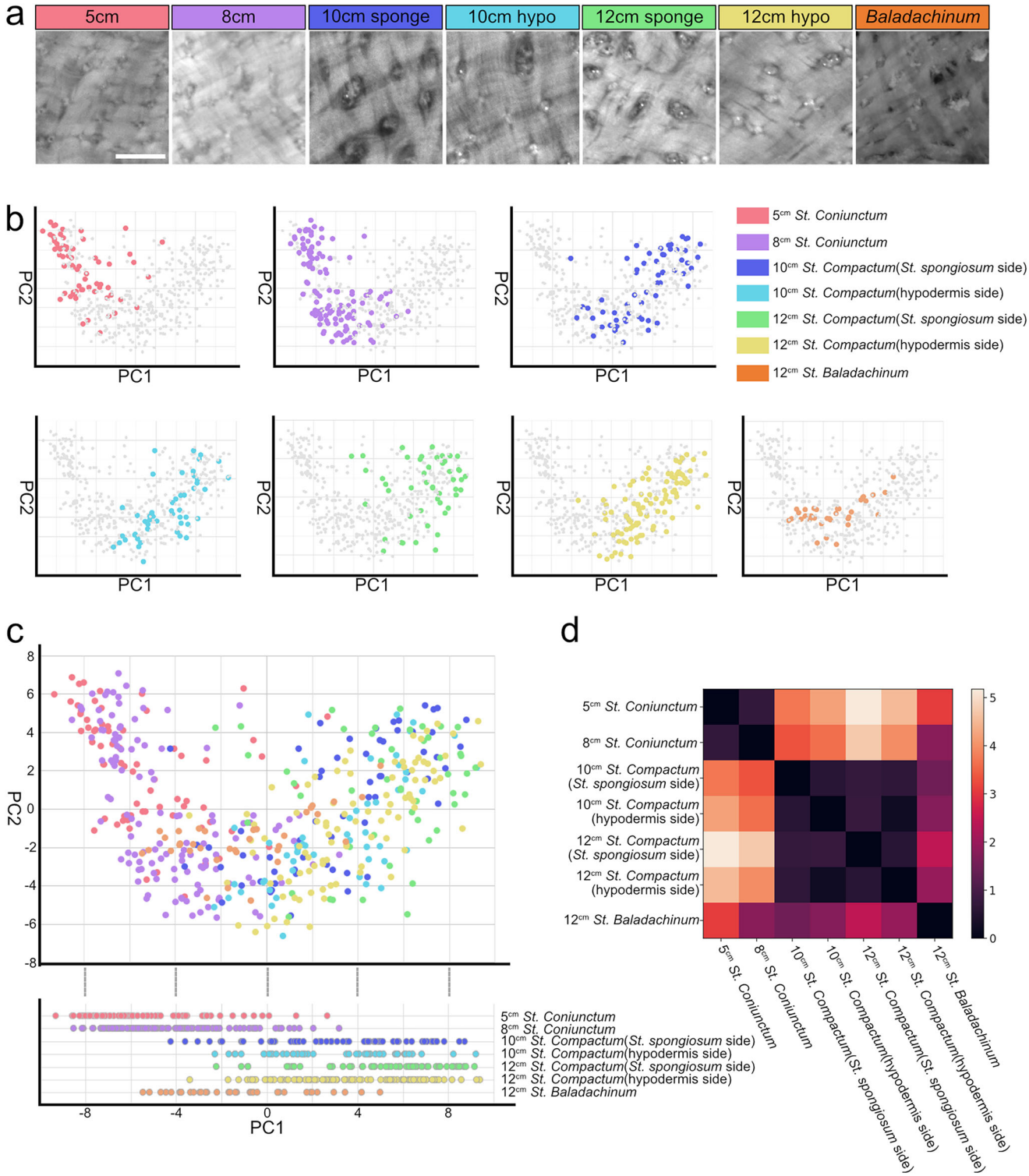

Fig. 8 | Analysis of structural changes in lattice-like collagen due to the involvement of lattice-patterned fibroblasts. a Representative images used for analysis. All images are the same magnification. The most representative image is shown from more than 30 images obtained from $n = 5$ biologically independent samples. **b**, **c** Principal components analysis (PCA) on features extracted using ResNet50. **b** PCA plot for each group; **c** PCA plot for all groups. **d** Heatmap of the effects of the Mahalanobis distance for seven groups. All images used for this analysis was registered in Dryad. Source data are provided as a Source Data file.

a gradual change in collagen fiber structure with growth from *stratum coniunctum* to SC. The scores of the SB of the 12 cm dermis are plotted between the *stratum coniunctum* and SC (Fig. 8c). This suggests that the SB in the 12 cm dermis receives some modification after lattice-patterned collagen production by keratinocytes. We further investigated structural similarities by measuring the distance between each cluster (Fig. 8d). The seven types of fibers could be classified into three groups: 5 and 8, 10, and 12 cm, and SB (Fig. 8d). Notably, SB exhibited a fiber structure distinct from that of SC and *Stratum coniunctum* (5 and 8 cm). However, when examining SB, it shared characteristics with 10 cm SC-Spo and 8 cm. Given that SB formation occurs after 10 cm, it is likely shaped following modifications by lattice-patterned

https://doi.org/10.1038/s41467-025-57055-7

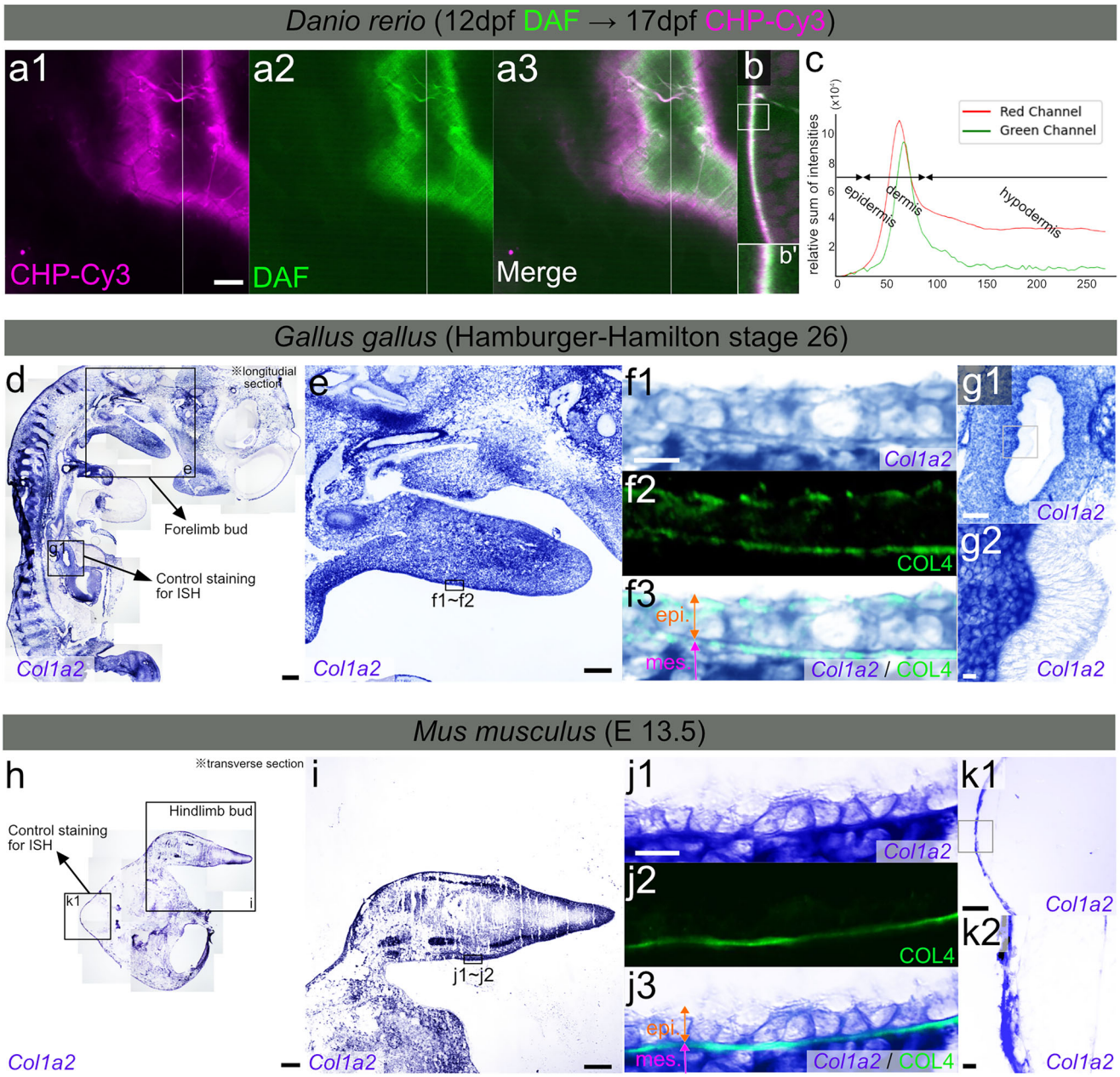

Fig. 9 | Type I collagen production by epidermal cells by various animal species. **a**–**c** Pulse-chase experiments with *Danio rerio*. **a** DAF and CHP-Cy3 signals at the epithermal side. **a1** CHP-Cy3, **a2** DAF, **a3** The marge image in (**a1**, **a2**). **b**, **b′** Orthogonal view from the reconstituted confocal microscopic images. **c** The histogram of relative sum of brightness. **d**–**g** Hamburger–Hamilton stage 26 embryo in *Gallus gallus domestics* **d** *Col1a2* gene expression pattern in the whole body section, **e** in the forelimb bud. f High magnification view in E. **f1** *Col1a2* gene expression pattern. **f2** Immunofluorescence of COL4. **f3** The Merge image of (**c1**, **c2**). **f1**–**f3** are the flipped images of the boxed region in (**e**). **g1** The negative control in the ectoderm. **g2** High magnification view in (**d1**). **h**–**k** Stage of E13.5 in *Mus musculus*. **h** *Col1a2* gene expression pattern in lower body section, **i** in the hindlimb bud. **j** High magnification view in (**f**). **j1** *Col1a2* gene expression pattern. **j2** Immunofluorescence of COL4. **j3** Merge images of 1 and 2. **j1**–**j3** are the flipped images of the boxed region in (**i**). **k1** The negative control in backbone. **k2** High magnification view in (**k1**). The **d**–**k** (exclude **f2**, **j2**) used pseudo-coloring. In **f3** and **j3**, epi. and mes. indicate epidermis and mesenchyme. The scale bars in a, **f1**, **g2**, **j1**, and **k2** are 10 μm, **d**, **h** are 500 μm, **e**, **i** are 100 μm, **g1** and **k1** are 100 μm. The results were confirmed in five biologically independent samples and experiments. Source data are provided as a Source Data file.

fibroblasts. Therefore, the strong structural similarities between 10 cm SC-Spo and 8 cm are logical, and the low similarity with 5 cm, which is solely formed from keratinocytes, is expected. These findings support the idea that the 5 cm lattice structure is gradually transformed into a 12 cm SC lattice structure by lattice-patterned fibroblasts.

Collagen production by epidermal cells in other species

Finally, to investigate whether collagen production in epidermal cells is a conserved mechanism in other animal species, we first performed pulse-chase experiments in zebrafish (Fig. 9a, b). DAF staining of zebrafish at 12 dpf was performed according to the method described before[14]. The DAF-stained zebrafish were then fixed at 17 dpf and stained with CHP-Cy3, thereby conducting a pulse-chase experiment like that shown in Fig. 5. The CHP-Cy3 signal was observed over a broader area than the DAF signal (Fig. 9a1–3). Similar to our findings in axolotls, the accumulation of new collagen (CHP-Cy3^{+} fibers) on the apical side was apparent when the reconstituted confocal image was observed orthogonally (Fig. 9b, b′). The procollagen signals were also

observed in epidermal cells, suggesting that the epidermal cells are a potential source of collagen even in zebrafishes (Supplementary Fig. 9a, a'). The quantification of the image in Fig. 9b is shown in Fig. 9c, confirming that the CHP-Cy3$^+$ region is shifted epidermal side. This result confirmed that new collagen is layered on the epidermal side in zebrafish. Next, we examined the pattern of *Col1a2* expression using different developmental stages of chicks and mice. We conducted in situ hybridization (ISH) and double staining with immunofluorescent staining for COL4 in chicks at stage 26 (Hamburger–Hamilton) (Fig. 9d–g). *Col1a2* signals were expressed in epidermal cells (Fig. 9d–f). A strong signal of *Col1a2* was visible in cells on the mesenchyme side. The COL4 signal could be observed at the mesenchyme–epidermis interface (Fig. 9f2). This could be a signal of COL4 in the basement membrane. The merged image is shown in Fig. 9f3, and control stains are shown in Fig. 9g1 and g2. A *Col1a2* signal could be observed inside the epidermal cells just above the COL4 signal in the immunofluorescence staining (Fig. 9f1–f3). Similar observations were made in mice (E13.5). In mice, as in chickens, a strong *Col1a2* signal could be observed on the mesenchyme (Fig. 9h–j). The results of *Col1a2* in epidermal cells and immunofluorescence of COL4 are shown in Fig. 9J1 and J2. The control staining is shown in Fig. 9k1 and k2. The *Col1a2* signal was observed in the epidermal cells just above the basement membrane in Fig. 9j3. The results of immunofluorescence using the procollagen antibody were shown in Supplementary Fig. 9b, b'. Similar to the ISH results in Fig. 9j, the procollagen signal could also be observed within the epidermal cells. These results suggest that epidermal cells are producing collagen even during the fetal stage of mammals. Therefore, these findings suggest that in various animal species, not only mesenchymal cells but also epidermal cells may produce type I collagen at the developmental stage.

Discussion

Keratinocyte-based dermal collagen formation

In this study, we demonstrated that the dermal collagen structure in the axolotl was formed by the cooperative activity of keratinocytes and mesenchymal cells (fibroblasts). Keratinocyte-based dermal collagen production had been speculated in previous studies[11,29]. In those studies, collagen production by keratinocytes was assumed based on the observation of collagen production in environments with few or no mesenchymal cells. Our data more directly demonstrated that keratinocytes are the primary source of dermal collagen in the early phase of axolotl skin development. Our result may help change the widely held view that keratinocytes do not produce collagen. Our results clearly indicate that collagens produced by the keratinocytes contribute to the dermis of the axolotl throughout their lifespan.

If the collagen production ability of keratinocytes is focused, it is possible to find that other types of collagen are produced by epithelial cells[30]. Potentially, no genetic regulatory mechanism is shared. However, given the intracellular trafficking of collagen molecules[31,32], it is likely that the trafficking system remains active in keratinocytes. This also supports the finding that keratinocytes of axolotls, zebrafishes, chicken embryos, and mouse embryos produce type I collagen.

Dermal collagen formation in axolotls

In the present study, we newly identified two dermal layers in addition to the two layers already determined. The *stratum coniunctum* is a monolayer formed transiently from collagens during axolotl dermal development (Fig. 3a, c). The SB is the uppermost layer in the relatively mature axolotl dermis (Fig. 3j). Collagens up to the 5 cm dermis stage appear to be synthesized mainly by keratinocytes, not dermal fibroblasts. In the 5 cm dermis, collagens were stacked apically (Fig. 5d), and filopodia from the fibroblasts (lattice-patterned cells) could not be observed (Fig. 3m). In contrast, we also observed *Col1a1*$^+$ cells underneath the *stratum coniunctum* (Fig. 4a, b). The presence of *Col1a1*$^+$ cells is thought to contribute to the formation of the pillar-like structures in the *stratum coniunctum* (Fig. 6a'). These pillar-like structures extend from the basal side of the *stratum coniunctum* toward the apical side (Fig. 6a'). At the 5 cm dermis stage, these structures are not observed (Fig. 3a, a'), and it is thought that the pillar-like structures are formed between the 5 and 8 cm dermis through collagen supply from basal *Col1a1*$^+$ cells. However, we have not addressed the role of basal *Col1a1*$^+$ cells at a stage earlier than 5 cm dermis. Consequently, the role of fibroblasts in the early phases of development warrants further investigation. In the later stage, the *stratum coniunctum* became thicker and the mesenchymal cells could be observed between the epidermis and the *stratum coniunctum* (8 cm dermis) although no mesenchymal cell could be observed there in the earlier stage (5 cm dermis) (Fig. 2q, r). Given that no major collagen stacking takes place in the hypodermal side in the transition of the dermis from 5 to 8 cm, the mesenchymal cells between the epidermis and the *stratum coniunctum* likely invade through the *stratum coniunctum*. We found that some of those are *Mmp2*$^+$ cells (Supplementary Fig. 4). This gene expression pattern also supports cell invasion through the collagen layer. This cell emergence may contribute to the separation of the dermal collagen layer into three layers (Figs. 2, 3). Regarding SS formation by migrating cells, the inhibition of fibroblast migration in wounded axolotl skin results in impaired SS thickening[11]. It is likely that invading cells play a similar role in the development of the SS in developing axolotl skin. However, it is still unclear whether cell invagination is the major force separating the SB and SC, because elimination of fibroblasts throughout skin development is currently impossible in axolotls. After the separation of the three layers, it is difficult to imagine that keratinocytes affect the lower layers, such as the SC. Given the *Col1a1* expression pattern, keratinocytes seem to produce less collagen after the separation of the three layers (Fig. 4d). Nevertheless, the newly synthesized collagens emerged throughout the dermis (Fig. 6a–l). This suggests that the center of collagen production shifts from the keratinocytes to the mesenchymal cells, and this shift might be conserved among species. We demonstrated the conserved collagen production mechanism by keratinocytes in mouse, chick, and zebrafish embryonic skin (Fig. 9). Generally, it is recognized that keratinocytes in the mature mammalian skin lose their ability to produce collagen and fibroblasts take on the role[20,21]. However, our findings suggest that the shift in collagen production from keratinocytes to mesenchymal cells (fibroblasts) appears to be a highly conserved evolutionary mechanism. Consequently, the axolotl dermal collagen system presents a valuable model for studying the developmental mechanisms of dermal collagen production across species.

Ultrastructure of the dermal collagen and the role of fibroblasts

Dermal collagen structures in the axolotl were investigated using EM. The ultrastructure of axolotl dermal collagen fibers appears to have a nested pattern (Supplementary Fig. 3), which results in the characteristic lattice-patterned collagen network[12]. We also clarified the spatial relationship between the basement membrane, collagen fibers, and keratinocytes (Supplementary Fig. 7). Not much is known about the basement membrane of axolotls. However, we could confirm the presence of the *lamina lucida* and *lamina densa*, suggesting that the basic structure of the basement membrane is conserved. Given the collagen production ability of keratinocytes, it is quite intriguing how collagen molecules go through the basement membrane. We confirmed the presence of laminin and COL4 in the axolotl basement membrane[9]. The basement membrane composed of these commonly conserved molecules may knit a loose network, or specific molecules may help the collagen molecules to pass through, or the orthodox structure of the basement membrane might allow collagen transfer. This is possible because a single unit of collagen is about 300 nm long and 1.5 nm in diameter[33], and it has been shown that albumin, which is about 4 nm in diameter[34], can pass through the glomerular basement

membrane. Furthermore, we observed the gap-like structure in our EM image (Supplementary Fig. 7e). Such holes in the basement membrane can be found in mouse and Drosophila embryos[23,24]. It has also been reported that there are holes in the basement membranes of adult mammalian skin, serving as pathways for immunocytes[35]. These findings suggest that the collagen molecule could potentially go through, and the basement membrane might function to arrange and orient the collagen. We cannot currently visualize collagen molecules passing through the basement membrane, but this should be investigated in the future.

EM revealed the unique relationship between lattice-patterned cells and collagen fibers. Lattice-patterned fibroblasts inserted filopodia just between warp and weft (Supplementary Fig. 3), consistent with previous findings that the lattice-patterned filopodia extended from cells and contributed to knitting collagen fibers in the SC[12]. Given the collagen production in those cells, it is reasonable that the role of lattice-patterned fibroblasts in the axolotl SC is the modification and maintenance of the collagen network originally produced by keratinocytes. Our results suggest that two patterns contribute to SC modification and maintenance: (1) the generation of new fibers, and (2) the thickening of existing fibers. The pulse-chase labeling technique using DAR and DAF revealed a slight shift to newly synthesized collagen fibers from older ones (Supplementary Fig. 8e, f), such that new fibers were added on the side of older fibers. Regarding the thickening of the existing fibers, EM observations clearly indicated that fibroblasts play a role in the process (Fig. 7). However, the biological and physiological meanings of modification by fibroblasts are still unknown. Furthermore, it is unclear whether fibroblasts can generate lattice-patterned collagen fibers without a lattice-patterned collagen template. Elucidating how existing collagen fibers interact with fibroblasts and the biological significance of this will help to confirm the mechanisms when collagen synthesis by keratinocytes has disappeared.

Lattice-patterned collagen networks without mesenchymal cell (fibroblast) participation

We clarified that the lattice-patterned collagen network was formed without or with minimum influence of mesenchymal cells (Figs. 3a, 5). The mechanism of how the lattice pattern is generated has been unknown, but there are some possibilities: (1) autonomous lattice formation of collagen molecules; (2) physical force by movement; or (3) directional filtration by the basement membrane. Collagens are rod-shaped molecules and can self-assemble. This molecular property may be sufficient to form a lattice pattern. To ensure this, a finer design of molecular simulation is necessary. Physical force should be part of the force to make a lattice pattern. An axolotl can move its limbs both intentionally and unintentionally, and such movement should generate a stretch force in the collagen fibers. It is well known that one-directional stretching contributes to aligning fibers. Aligning the collagen molecules via filtering by the basement membrane is another possibility. As mentioned above, collagen molecules may be able to pass through the basement membrane vertically. This selection in molecular orientation may reasonably account for collagen alignment. However, there is no clear explanation as to why the collagen fibers make the characteristic lattice pattern in the axolotl dermis. The process by which geometrically ordered forms are created by amorphous cells is a very interesting biological topic. More sophisticated observation methods and simulations will help to solve the problem. Elucidating the process of well-ordered collagen formation may lead to a technique whereby complete regeneration of the skin without scar formation is possible.

Perspectives on dermal collagen formation

Dermal collagen, a crucial component of skin structure, has long been attributed solely to fibroblast production in mammals. However, the in vivo dynamics of dermal collagen construction have remained elusive, primarily due to the opacity of mammalian skin. The axolotl, with its remarkable skin transparency, offers an unprecedented opportunity to revise our understanding of dermal collagen architecture. Leveraging the unique transparency of axolotl skin, we conducted an in-depth investigation into the process of dermal collagen formation. Our findings are summarized in Fig. 10, illustrating the detailed process of axolotl dermal collagen formation.

These findings reveal that axolotl dermal collagen is the result of intricate spatiotemporal coordination among diverse cell types, collectively constructing a complex three-dimensional collagen framework. Importantly, our research highlights a paradigm shift:

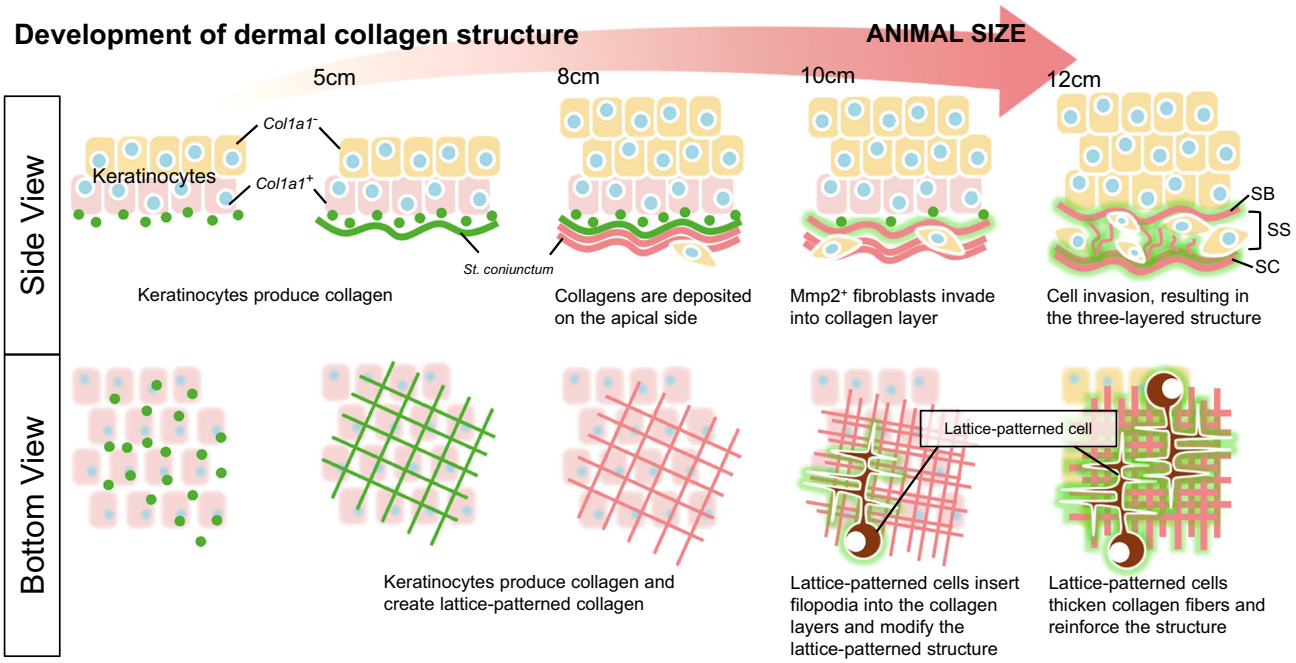

Fig. 10 | Summary of dermal collagen development in *Ambystoma mexicanum*. The upper section shows a cross-sectional view of the axolotl dermal collagen formation process. The lower section shows the same process viewed from a planar perspective.

keratinocytes play an important role in the early stage of lattice-patterned collagen structure formation. This paradigm-shifting model offers a new foundation for understanding vertebrate dermal collagen formation and holds significant potential for advancing regenerative medicine and skin bioengineering.

Methods

Animals

Axolotls (*Ambystoma mexicanum*) were procured from the Hiroshima University Amphibian Research Center and kept in aerated water at 22 °C. The leucistic strain was used in all experiments. For the surgical experiments conducted in this study, axolotls with nose-to-tail lengths ranging from 5 to 12 cm were used, with no specific bias towards either sex. The care and treatment of the animals in this study was carried out under protocols approved by the Animal Care and Use Committee of Okayama University. All animal experiments adhered strictly to the guidelines provided by the Animal Care and Use Committee of Okayama University. Every possible measure was taken to minimize animal suffering, in line with the NIH Guide for the Care and Use of Laboratory Animals. Zebrafish (*Danio rerio*) were originally obtained from the Zebrafish International Resource Center. The individuals bred in our laboratory were used for the experiments. Regarding the ddY mouse embryo, and chick embryo, the fixed samples were bought from companies (mouse:Tokushima Molecular Pathology Institute, Inc, chick: alphabio, Inc).

Histology

Harvested limbs were fixed in 4% paraformaldehyde (PFA) in phosphate-buffered saline (PBS) at room temperature overnight. To prepare frozen sections, fixed samples were decalcified in 10% EDTA at room temperature overnight, equilibrated in 30% sucrose in PBS at room temperature overnight, and frozen in O.C.T. compound (Sakura Finetek). Frozen sections were cut to a thickness of 12 µm using a CM1850 cryostat (Leica) and dried. Collagen fibers were visualized using a Masson's Trichrome Stain Kit (HT15-1KT, Sigma). Masson's trichrome staining was performed as follows. The prepared frozen sections were washed with water and post-fixed in preheated Bouin's solution at 65 °C for 15 minutes. After post-fixation, the sections were washed with water and stained with Weigert's hematoxylin solution at room temperature for 15 min. Following a water wash, fuchsin solution was applied to the sections, which were stained at room temperature for 3 min and washed again with water. Next, a phosphomolybdic-phosphotungstic acid solution was applied and reacted at room temperature for 5 min, followed by staining with aniline blue at room temperature for 5 min. Finally, the sections were washed with 100% ethanol and G-NOX and mounted with a soft mounting solution (Softmount, Fuji Film). Elastic fibers were visualized using a Victoria Blue stain solution (Muto Pure Chemicals Co., Ltd, 40772). Victoria Blue staining was performed as follows. The frozen sections were first washed with water and then with 95% ethanol. The sections were stained with Victoria Blue stain solution at room temperature for 2 min, followed by a wash with 70% ethanol and replacement with water. Finally, the sections were mounted in glycerin. Images were acquired using a BX61 microscope (Olympus).

Collagen visualization

To visualize the fibers of type I collagen in the forelimb at the dermal skin, we used DAR-4M (SK1005-01, Goryo Chemical) and DAF-FM DA (SK1004-01, Goryo Chemical). Each solution (1–2 µL) was injected under the skin of an axolotl dorsal limb using a fine glass capillary. One day later, injected skin was harvested and fixed by 4% paraformaldehyde (PFA) in phosphate-buffered saline (PBS) at room temperature overnight. The fixed skin sample was washed with Tris-buffered saline with Tween 20 (TBST) and stained for nuclei using DAPI solution (19178-91, 5 µg/mL, Nakarai tesque) and tissue clearing using CUBIC-R + (N) (Tokyo Chemical Industry), and the samples were mounted in Mounting Solution (PI 1.520) for CUBIC-R+ (Tokyo Chemical Industry). Images were acquired using a FV3000, and FV4000 confocal laser scanning microscopes (Evident). To visualize the structure of the *stratum baladachinum*, maximum intensity projection was applied to the confocal images using Fiji software. Normalization and adjustments of brightness and contrast were applied to figure images using Fiji software. Three-dimensional construction of collagen and cell structure was performed using Amira software. Deconvolution (Supplementary Fig. 8e) was performed using cellSense software (Evident).

Measurement of the region of interest in Z-stack images

We measured the area of GFP $^+$ filopodia in the SC (Fig. 3m) using Fiji software. We used the image set in which Type I collagen in the CMV::GFP transgenic axolotls was stained with DAR-4M. To measure the area of filopodia, we isolated the SC region. This extraction was limited to the GFP (green) channel. The green channel (GFP) was then converted to grayscale, and normalization was applied using the Fiji Plugin (normalization local contrast). Then, we set the threshold for the green channel (GFP) to 40–125, selecting the GFP $^+$ area within this range. The GFP $^+$ area was further limited to regions containing only lattice-patterned filopodia, and both the selected GFP $^+$ area and the total area of the selected region were measured. This method was applied to all Z-stack images of the isolated SC. We analyzed more than 15 images taken from $n = 3$ biologically independent samples, with each point on the box plot representing the result from one image analysis. Similarly, the red and green area measurements (Figs. 5, 6 and Supplementary Fig. 6) were conducted in Fiji. Z-stack image color channels were separated and converted to grayscale. Each channel's Z-stack images were normalized using the previously mentioned Fiji. For the normalized Z-stack images, we set the threshold to 45–255 and selected signals within this range. The selected area was then measured across all Z-stack images to quantify the red and green areas.

Analysis of collagen fiber orientation

To investigate fiber orientation, the directionality plugin of Fiji was used: a Z-stack image of collagen visualized using DAF/DAR was converted to greyscale, and a 200-pix-square region was extracted for analysis. Normalization processing was applied to the extracted images using Fiji, and Fourier components were calculated using the directionality plugin.

Immunofluorescence

The following primary antibodies were used for immunofluorescence staining: rabbit anti-GFP pAb (MBL Cat# 598, 1:500, RRID:AB_591819), mouse anti-collagen type I (#C2456-2 ML, 1:500; Sigma), mouse anti-pan cytokeratin (AE1 + AE3) antibody (NBP2-29429, 1:100; Novus Biologicals), mouse anti-procollagen type I aminoterminal extension peptide (SP1.D8, 1:10; DSHB), rabbit anti-Laminin (L9393, 1:100; Sigma), rabbit anti-collagen type III alpha1 (N-terminal) (22734-1-AP, 1:500; Proteintech), rabbit anti-collagen type IV (600-401-106-0.1, 1:100; Rockland), rabbit anti-procollagen type I (orb389309, 1:100; Biorbyt) and mouse anti-collagen Type2 (II-II6B3C, 1:100; DSHB).
Antigen retrieval was performed for mouse anti-procollagen type I aminoterminal extension peptide and rabbit anti-procollagen type I antibodies. Antigen retrieval and Proteinase K (25530049, Invitrogen, 5 µg/ mL) digestion at room temperature for 30 min were performed for mouse anti-collagen type I, rabbit anti-laminin, rabbit anti-collagen type IV, and mouse anti-collagen type II antibodies. The secondary antibody was the anti-mouse IgG Alexa 488 conjugated antibody (A11017, 1/1000; Invitrogen), goat anti-rabbit IgG Alexa 594 (A-11012, 1:1000; Invitrogen), and anti-rabbit IgG Alexa 488 (Cat# A-21207, RRID: AB_141637, 1:500, Thermo Fisher). The nuclear staining was performed using Hoechst 33342 (19172-51, 0.125 µg/ mL, Nacalai tesque). Images were acquired using a BX61 microscope (Olympus) and an FV3000

confocal laser scanning microscope (Evident). To visualize the structure of an entire single cell, maximum intensity projection was applied to the confocal images using Fiji software. Adjustments of brightness and contrast were applied to the figure images using Fiji software. The heatmaps (Fig. 4e′–h′) were created using Fiji. We converted RGB images to grayscale. The heatmap was created using Fiji's look-up table (16 colors) for a grayscale image. The original images used to create the heatmaps were taken under the same image-capturing conditions. The integrated heatmap was created by processing the captured images using Python code. Briefly, the images were measured at multiple distances between two points that traverse the collagen layer of the dermis, and the Col1a signal intensity between the two points was calculated. Data from the same dermal developmental stage were then standardized to the mean value of the distance between those two points. The mean values of all intensities were rearranged to the mean value of the two conversion distances and displayed as a heatmap. The code necessary for a series of integrated analyses has been registered and published on GitHub (https://doi.org/10.5281/zenodo.14729473).

Measurement of collagen layer thickness and number of nuclei

To measure the thickness of the collagen layer (Fig. 2u), images of sections immunofluorescence stained with type I collagen were converted to greyscale; normalization was performed using Fiji's Normalization to obtain binarized data. The length (pix) of any ten points from the binarized data was measured. From each of the $n = 4$ independent samples, two images were acquired, and ten measurements were taken per image. Each point on the box plot represents all measured data points. To count the number of nuclei (Fig. 2v), binarized images of sections immunofluorescence stained for type I collagen were acquired in the same way and superimposed with Hoechst staining. For the independent samples ($n = 4$ for 5 cm; $n = 5$ for 8, 10, and 12 cm), two images were obtained and analyzed per sample. Each point on the box plot represents all measured data points. The number of nuclei present inside the collagen layer was measured using a Fiji cell counter.

In situ hybridization

Axolotl *Mmp2*, axolotl *Mmp9*, axolotl *Mmp14*, chick *Col1a2*, and mouse *Col1a2* were isolated by reverse transcription polymerase chain reaction (RT-PCR) using the following primers: *Mmp2* forward, AAGAAGCCTCGCTGTGGTAA and *Mmp2* reverse, ATCAGGGACACCAGTCCAAG; *Mmp9* forward, GCGCACGATGTCTTTCTGTA and *Mmp9* reverse CTTCCCTCTCTTGCCACTTG; *Mmp14* forward, TGAGACCTATGAGGCCATCC, and *Mmp14* reverse; CAGTCACGCAGCACAGATTT, Chick *Col1a2* forward, GAGGTGAACCTGGCAACATT and Chick *Col1a2* reverse CTGCATCAAAGCCAACTTCA; mouse *Col1a2* forward GACATGCTCAGCTTTGTGGA and reverse, ACCTTTGCCACCTTGAACAC; and axolotl *Col1a1* and *Mmp1*, as previously described[36,37]. The isolated genes were subcloned into the pTAC2 vector and sequenced. Probe synthesis was performed by T7 or SP6 RNA polymerase. Regarding *Mmp13*, the gene could not be isolated by RT-PCR. Thus, the sequence of its open-reading frame region was synthesized (Eurofin). Section in situ hybridization was performed as previously described[38]. Images of axolotl tissues were acquired using a BX61 microscope (Olympus). Images for mouse and chick tissues were taken by confocal microscope (FV3000, Evident). The color was applied after taking pictures with a monochrome camera by Fiji or Photoshop CS6.

Immunoelectron microscopy

Sample for immunoelectron microscopy (IEM) samples were immersion-fixed with 4% paraformaldehyde PBS overnight at room temperature. Preparations were dehydrated through increasing concentrations of methanol, embedded in LR Gold resin (Electron Microscopy Sciences), and polymerized under UV lamps at −20 °C for 24 h. Immunoelectron microscopy was performed as described previously[39]. Briefly, ultrathin sections (70 nm thick) were collected on nickel grids that were coated with a collodion film, rinsed with phosphate-buffered saline (PBS) several times, and then incubated with 2% normal goat serum and 2% BSA in 50 mM Tris(hydroxymethyl)-aminomethane-buffered saline (pH 8.2) for 30 min to block non-specific binding. To detect Procollagen signals in tissues, To detect Procollagen signals in tissues, a 1:1 solution of undiluted mouse anti-procollagen antibody (DSHB, Cat# SP1.D8) and Can Get Signal Solution 1 (TOYOBO) was used to incubate the sections for 1 hour at room temperature. This was followed by incubation with a biotinylated goat anti-rabbit IgG antibody, and then with an avidin-biotin-HRP complex using a streptavidin-biotin intensification kit (Nichirei). Finally, a goat anti-HRP antibody conjugated to 12 nm gold particles (Jackson Immuno Research Laboratory, West Grove) was applied. The sections were then viewed using an H-7650 electron microscope (Hitachi).

Epoxy resin was used to observe the tissue structure. The skin samples were immersed in 4% paraformaldehyde and 2% glutaraldehyde in PBS overnight at room temperature, washed with 0.1 M Phosphate Buffer Solution (PB), then post-fixed with 1% osmium tetroxide in 0.1 M PB for 2 h at room temperature. The skin samples were washed with 0.1 M PB, dehydrated, and embedded in epoxy resin (Quetol-812; Nisshin EM, Tokyo, Japan). Ultrathin sections were prepared as described above.

Thickness measurement of single collagen fibers

Normalization was performed on the images obtained from the electron microscope, and the images were binarized. A median was applied to the binarized images. To separate each fiber, the watershed function of Fiji was applied, and the fiber area was measured using Fiji's "Analyze particle". Three biologically independent samples ($n = 3$) were analyzed, and two images were obtained and analyzed per sample. Each point on the box plot represents all measured data points.

Analysis of lattice-patterned collagen fiber

For low-dimensional visualization of the collagen image dataset, we manually cropped image patches (200 × 200 pixels) without overlap from the confocal images of collagen fibers. To ensure a focused analysis of the collagen fiber pattern, we excluded regions without collagen due to cell invasion and extracted only areas limited to the lattice structure. This produced 484 grayscale images. For transparency and reproducibility, all images have been uploaded to Drayd (https://doi.org/10.5061/dryad.6q573n66z). As the first step of dimension reduction (from 200 × 200-pixel intensities to 2048-dimensional feature vector), the images were input into a deep-learning model for image recognition, ResNet50 with ImageNet-pretrained weights (ResNet50_Weights.IMAGENET1K_V2 from the torchvision library) for feature extraction. We extracted image features from the last global average pooling layer. Then, linear PCA was applied to the 2048-dimensional feature vectors. We performed no training of the neural network with our data; hence, the feature extraction was agnostic on which developmental stages the images came from. To quantify distances between the clusters in the low-dimensional space, we adopted the Mahalanobis distance. First, we computed $\mathbf{M}$, where M_{ij} represents the Mahalanobis distance from the mean of ith cluster to jth cluster. Then, we symmetrized it as $\mathbf{D} = (\mathbf{M} + \mathbf{M}^{\mathrm{T}})/2$ (Fig. 8).

Plasmid transfection and transgenic

To visualize the fibers of type I collagen in dermal skin, we designed a GFP-Col1a2 plasmid vector containing a CMV promoter-secretory signal-$(Gly_4Ser)_3$ linker-AcGFP-$(Gly_4Ser)_3$ linker-Col1a2-SV40 poly A signal based on pCS2 plasmid. For visualization of cell morphology, we used an mCherry plasmid vector containing a CMV promoter-mCherry-SV40 poly A signal based on the pCS2 plasmid. The plasmids were purified by CsCl-EtBr ultracentrifugation and prepared in a 1.5 μg/μL concentration. Plasmid solution (0.4–2 μg/μL) was mixed with Fast Green dye for

visualization and injected under the skin of an axolotl limb using a fine glass capillary. Immediately after injection, electric pulses were applied (20 V, 50 ms pulse length, 950 ms interval, ten times).

To create transgenic axolotls, we subcloned GFP-Col1a2 into the pIsceI vector (a gift from T. Hayashi). The plasmid was purified using cesium chloride gradient centrifugation. The generation of transgenic axolotls followed a previously published method (PMID: 25740493; https://doi.org/10.1111/dgd.12019). F1 transgenic animals were used for the experiments.

Pulse-chase observation of the collagen fibers in zebrafish dermis

Living larval zebrafish at 12 days post fertilization (dpf) were incubated in a solution of 5 µM DAF-FM DA (diluted in tank water) at room temperature for 12 h in the dark. After the incubation, the fish were immediately returned to fresh tank water and bred for 5 days. The fish were subsequently anesthetized with tricaine (MS-222) at an optimal concentration and fixed in 4% PFA at 4 °C overnight. After the fixation, the samples were washed with PBS and incubated for the denaturation of collagen fibers at 80 °C for 5 min. Finally, the samples were stained with 10 µM Collagen Hybridizing Peptide (CHP) -Cy3 (3Helix, FLU60) at 4 °C overnight, and after subsequent washing with PBS, they were observed by a confocal microscope, LSM 780 (Carl Zeiss). The quantification was performed using the Fig. 9b tiff image, with the original python code created and executed for the analysis (the original python code is provided in GitHub (https://doi.org/10.5281/zenodo.14729490).

Microscopes and image analysis

Confocal laser microscopy was performed using FV3000, FV4000 (Evident), and LSM 780 (Carl Zeiss). The objective lenses used for FV3000 and FV4000 were UPlanXApo 20x/0.80 and UPlanXApo 60x/1.42 Oil. For LSM 780, Plan-Apochromat 20×/0.8 M27 and C-Apochromat 40×/1.20 W Korr FCS M27 were used. For fluorescence microscopy using the BX61 (Olympus), the objective lenses UPlanFL 10x/0.3, UPlanXApo 20x/0.8, and UPlanXApo 40x/0.95 were used, and images were acquired with a color camera and long pass filter. Image analysis was conducted using Fiji and AMIRA software. Images were processed and arranged into figures using Photoshop CS6 or Affinity Photo (version 1.10.6.1665).

Statistics and reproducibility

We did not employ strict statistical methods to determine the sample size, but given the high reproducibility of the results, we considered these sample sizes to be sufficient. This study includes an analysis of multiple skin stages of axolotls. Consistent observations obtained from independent experiments performed at different skin stages support the sufficiency and reproducibility of our results (with sample sizes of at least $n = 3$ skins per experiment). No data were excluded from the analyses. We did not specifically distinguish between the sexes of the animals. This is because there is no evidence of gender-based differences in skin properties. The investigators were not blinded to allocation during the experiments or outcome assessment due to the nature of the sample preparation. However, to ensure the robustness of the statistical analysis, the results were independently verified by a different researcher who conducted the analysis with anonymized sample labels, and the same results were confirmed.

Reporting summary

Further information on research design is available in the Nature Portfolio Reporting Summary linked to this article.

Data availability

All codes used in this study are publicly available on GitHub. All other relevant data supporting the key findings of this study are available within the article and its Supplementary Information files or from the corresponding author upon request. The quantitative data used in this study are provided in the Source Data file. Source data are provided with this paper.

Code availability

All python code related to this manuscript is available on GitHub (https://doi.org/10.5281/zenodo.14729473; https://doi.org/10.5281/zenodo.14729490).

References

1. Tarnutzer, K., Siva Sankar, D., Dengjel, J. & Ewald, C. Y. Collagen constitutes about 12% in females and 17% in males of the total protein in mice. *Sci. Rep.* **13**, 4490 (2023).
2. Ogawa, R. & Akaishi, S. Endothelial dysfunction may play a key role in keloid and hypertrophic scar pathogenesis - Keloids and hypertrophic scars may be vascular disorders. *Med. Hypotheses* **96**, 51–60 (2016).
3. Chung, J. H. et al. Modulation of skin collagen metabolism in aged and photoaged human skin in vivo. *J. Invest. Dermatol.* **117**, 1218–1224 (2001).
4. Quan, T. & Fisher, G. J. Role of age-associated alterations of the dermal extracellular matrix microenvironment in human skin aging: a mini-review. *Gerontology* **61**, 427–434 (2015).
5. Haydont, V., Bernard, B. A. & Fortunel, N. O. Age-related evolutions of the dermis: clinical signs, fibroblast and extracellular matrix dynamics. *Mech. Ageing Dev.* **177**, 150–156 (2019).
6. Iriyama, S., Ogura, Y., Nishikawa, S., Hosoi, J. & Amano, S. Regeneration of collagen fibrils at the papillary dermis by reconstructing basement membrane at the dermal–epidermal junction. *Sci. Rep.* **12**, 795 (2022).
7. Osman, O. S. et al. A novel method to assess collagen architecture in skin. *BMC Bioinformatics* **14**, 260 (2013).
8. Abe, G. et al. Insights regarding skin regeneration in non-amniote vertebrates: skin regeneration without scar formation and potential step-up to a higher level of regeneration. *Semin. Cell Dev. Biol.* **100**, 109–121 (2020).
9. Seifert, A. W., Monaghan, J. R., Voss, S. R. & Maden, M. Skin regeneration in adult axolotls: a blueprint for scar-free healing in vertebrates. *PLoS ONE* **7**, e32875 (2012).
10. Yokoyama, H. et al. Skin regeneration of amphibians: a novel model for skin regeneration as adults. *Dev. Growth Differ.* **60**, 316–325 (2018).
11. Seifert, A. W., Cook, A. B. & Shaw, D. Inhibiting fibroblast aggregation in skin wounds unlocks developmental pathway to regeneration. *Dev. Biol.* **455**, 60–72 (2019).
12. Kashimoto, R. et al. Lattice-patterned collagen fibers and their dynamics in axolotl skin regeneration. *iScience* **25**, 104524 (2022).
13. Kashimoto, R. et al. FGF signaling induces the regeneration of collagen fiber structure during skin wound healing in axolotls. *Dev. Biol.* **498**, 14–25 (2023).
14. Kuroda, J., Hino, H. & Kondo, S. Dynamics of actinotrichia, fibrous collagen structures in zebrafish fin tissues, unveiled by novel fluorescent probes. *PNAS Nexus* **3**, pgae266 (2024).
15. Eyre, D. R., Apon, S., Wu, J. J., Ericsson, L. H. & Walsh, K. A. Collagen type IX: evidence for covalent linkages to type II collagen in cartilage. *FEBS Lett.* **220**, 337–341 (1987).
16. Olsen, B. R. Collagen IX. *Int. J. Biochem. Cell Biol.* **29**, 555–558 (1997).
17. Van Der Rest, M. & Garrone, R. Collagen family of proteins. *FASEB J.* **5**, 2814–2823 (1991).
18. Becker, J. et al. Immunoelectron microscopic localization of collagens type I, V, VI and of procollagen type III in human periodontal ligament and cementum. *J. Histochem. Cytochem.* **39**, 103–110 (1991).
19. Huang, Y. H., Ohsaki, Y. & Kurisu, K. Distribution of type I and type III collagen in the developing periodontal ligament of mice. *Matrix* **11**, 25–35 (1991).

20. Deng, C. C. et al. Single-cell RNA-seq reveals fibroblast heterogeneity and increased mesenchymal fibroblasts in human fibrotic skin diseases. *Nat. Commun.* **12**, 3709 (2021).
21. Ma, F. et al. Single cell and spatial sequencing define processes by which keratinocytes and fibroblasts amplify inflammatory responses in psoriasis. *Nat. Commun.* **14**, 3455 (2023).
22. Gelse, K. & Pöschl, E. Aigner T. Collagens–structure, function, and biosynthesis. *Adv. Drug Deliv. Rev.* **55**, 1531–1546 (2003).
23. Kyprianou, C. et al. Basement membrane remodelling regulates mouse embryogenesis. *Nature* **582**, 253–258 (2020).
24. Matsubayashi, Y. et al. A moving source of matrix components is essential for de novo basement membrane formation. *Curr. Biol.* **27**, 3526–3534.e3524 (2017).
25. Pokidysheva, E. N. et al. Collagen IV of basement membranes: II. Emergence of collagen IV(α345) enabled the assembly of a compact GBM as an ultrafilter in mammalian kidneys. *J. Biol. Chem.* **299**, 105459 (2023).
26. He K., Zhang X., Ren S. & Sun J. Deep residual learning for image recognition. In *2016 IEEE Conference on Computer Vision and Pattern Recognition* (*CVPR*) (IEEE, 2016).
27. Tomizawa, Y. et al. Harnessing deep learning to analyze cryptic morphological variability of *Marchantia polymorpha*. *Plant Cell Physiol.* **64**, 1343–1355 (2023).
28. Toulany, N. et al. Uncovering developmental time and tempo using deep learning. *Nat. Methods* **20**, 2000–2010 (2023).
29. Le Guellec, D., Morvan-Dubois, G. & Sire, J. Y. Skin development in bony fish with particular emphasis on collagen deposition in the dermis of the zebrafish (*Danio rerio*). *Int. J. Dev. Biol.* **48**, 217–231 (2004).
30. Oguchi, M., Kobayasi, T. & Asboe-Hansen, G. Secretion of type IV collagen by keratinocytes of human adult. *J. Invest. Dermatol.* **85**, 79–81 (1985).
31. Bonfanti, L. et al. Procollagen traverses the Golgi stack without leaving the lumen of cisternae: evidence for cisternal maturation. *Cell* **95**, 993–1003 (1998).
32. Chioran, A., Duncan, S., Catalano, A., Brown, T. J. & Ringuette, M. J. Collagen IV trafficking: the inside-out and beyond story. *Dev. Biol.* **431**, 124–133 (2017).
33. Shoulders, M. D. & Raines, R. T. Collagen structure and stability. *Annu. Rev. Biochem.* **78**, 929–958 (2009).
34. Farquhar, M. G. The primary glomerular filtration barrier—basement membrane or epithelial slits? *Kidney Int.* **8**, 197–211 (1975).
35. Oakford, M. E. et al. Migration of immunocytes across the basement membrane in skin: the role of basement membrane pores. *J. Invest. Dermatol.* **131**, 1950–1953 (2011).
36. Mitogawa, K., Makanae, A., Satoh, A. & Satoh, A. Comparative analysis of cartilage marker gene expression patterns during axolotl and xenopus limb regeneration. *PLoS ONE* **10**, e0133375 (2015).
37. Satoh, A., makanae, A., Hirata, A. & Satou, Y. Blastema induction in aneurogenic state and Prrx-1 regulation by MMPs and FGFs in Ambystoma mexicanum limb regeneration. *Dev. Biol.* **355**, 263–274 (2011).
38. Makanae, A., Mitogawa, K. & Satoh, A. Co-operative Bmp- and Fgf-signaling inputs convert skin wound healing to limb formation in urodele amphibians. *Dev. Biol.* **396**, 57–66 (2014).
39. Sakamoto, H. & Inutsuka, A. Membrane-targeted palGFP predominantly localizes to the plasma membrane but not to neurosecretory vesicle membranes in rat oxytocin neurons. *Acta Histochem. Cytochem.* **57**, 85–88 (2024).

Acknowledgements

We are grateful to Dr. James Monaghan for sharing valuable images. We also thank Ms. R. Iwata and T. Satoh for supporting office work and animal housing. We received intangible support from Olympus (Evident) in our work on collagen imaging, for which we are grateful to Mr. Takeshita (Okuma/Evident). We thank Dr. Y. Matubayashi of Bournemouth University, Dr. N. Funayama of Kyoto University, and Dr. R. Kashimoto for their valuable advice on our experiments. A.O. is grateful for a SUNBOR SCHOLARSHIP from the Suntory Foundation for Life Sciences and ANRI Basic Science Scholarship. This work was supported by the following funding sources: JSPS Kakenhi (A.S.: #20H03264, #24K02034, #23H04314, and #24H01953), Koyanagi Foundation (A.S.), JST SPRING (#JPMJSP2126 A.O.), and the National Institute for Basic Biology Collaborative Research Programs, Trans-Scale Biology (#22NIBB101 to A.S.), and Integrative Imaging (22NIBB506 to A.S.).

Author contributions

A.O. and A.S. contributed to building the concept of the experiment. The methodology was developed and established by A.O., H.S., J.K., Y.Kon., and A.S. All data validation was performed by A.O. A.O., S.F., and S.Y. contributed to animal housing. Imaging parts were taken by A.O., J.K., and Y.Kam. The original draft was written by A.S. and A.O. Then, all authors (A.S., A.O., H.S., J.K., Y.Kon., Y.Kam., S.N., S.F., and S.Y.) contributed to reviewing and editing the manuscript. A.S. and A.O. played a role in the funding acquisition.

Competing interests

The authors declare no competing interests.

Additional information

Supplementary information The online version contains supplementary material available at https://doi.org/10.1038/s41467-025-57055-7.

Correspondence and requests for materials should be addressed to Akira Satoh.

Peer review information *Nature Communications* thanks Jennifer Young, who co-reviewed with Huan Ting Ong and the other, anonymous, reviewer(s) for their contribution to the peer review of this work. A peer review file is available.